Microgravity Science and Technology (2022) 34: 6
https://doi.org/10.1007/s12217-021-09923-2

ORIGINAL ARTICLE

On the Space Thermal Destratification in a Partially Filled Hydrogen Propellant Tank by Jet Injection

Ji-Cheng Li[1,2] · Bin Guo[1,3] · Jian-Fu Zhao[1,3] · Kai Li[1,3] · Wen-Rui Hu[1,3]

Received: 28 July 2021 / Accepted: 14 December 2021 / Published online: 31 December 2021

Abstract

Hydrogen, as a space propellant, plays an important role in future space energy systems. However, it is sensitive to heat leakage from the environment because of its low boiling point and small density. Besides, the buoyancy convection is weakened and even completely suppressed in space microgravity environment. When there is heat leakage on the wall of the propellant tank, temperature stratification will be produced around the heat leakage source, resulting in propellant overheating. This will affect the interfacial heat and mass transfer, leading to pressure rise in the tank, and even endanger the structural safety of the system. To prevent tank pressure from rising above its design limits, venting or active pressure control techniques must be implemented. The cryogenic jet mixing is an effective method to suppress temperature stratification. The cryogenic fluid is mixed with the fluid inside the tank through a jet nozzle to reduce the thermal stratification and achieve uniform temperature distribution. In the present study, the temperature stratification phenomenon caused by heat leakage and its destratification via a cryogenic jet under microgravity condition were numerically investigated in the context of a partially liquid-filled large scale model tank. The effects of cryogenic jet mixing on the elimination of temperature stratification were analyzed for different initial filling ratios and mass flow rates. The results show that a higher incident mass flow rate can effectively destroy the temperature stratification inside the tank and promote an inside fluid flow for a given liquid filling ratio. A smaller filling ratio results in a faster growth in both average temperature and average pressure, and a larger amount of mass transfer inside the tank. It is more efficient to implement the cryogenic jet injection in the early stage when the remained propellant is still abundant, or adopt a higher incident mass flow rate to suppress the thermal stratification in the tank.

Keywords Microgravity · Thermal destratification · Cryogenic jet mixing · Two-phase flow

Introduction

Liquid Hydrogen (LH2), as a widely used space propellant, plays an important role in the future energy system. However, it is sensitive to occur heat leakage from the environment because of its low boiling point. In a partially filled propellant tank, the phenomenon of gas/liquid two-phase flow inside the tank is complicated under microgravity conditions. Capillary force becomes the major factor, resulting in an uneven distribution of the two-phase flow field and irregular interface morphology. Moreover, when there is a local heat leakage on the wall of propellant tank, temperature stratification arises around the heat leakage source. This will cause local overheating, and will also seriously affect the multiphase heat and mass transfer in the propellant tank, which will raise the tank pressure and endanger the structural safety of the system. The cost of space experiments on cryogenic propellant tank is tremendously high. Therefore, thermal stratification in storage tanks was mainly studied by terrestrial experiments and theoretical analyses in the early stage. Schmidt et al. (1961) carried out on-ground experiments in a Dewar bottle of 625 gallons in volume. The thermal field were measured for different pressure levels, pressurization gas consumption and ullage pressure, and a thermodynamic analysis method was presented to investigate the mechanism of heat transfer and thermal desorption inside the LH2 storage tank. Barnett et al. (1965) adopted a

✉ Kai Li
kai.lee@imech.ac.cn

[1] National Microgravity Laboratory, Institute of Mechanics, Chinese Academy of Sciences, Beijing 100190, China

[2] School of Energy and Power Engineering, Lanzhou University of Technology, Lanzhou 730050, China

[3] School of Engineering Sciences, University of Chinese Academy of Sciences, Beijing 100049, China

semi-empirical method for analyzing the convective boundary layer and the observed hyperbolic temperature profile distribution and predicting the thermal distribution inside the tank. Aydelott (1967a, 1967b, 1969) carried out experimental investigations on a spherical LH2 storage tank in gravity conditions. Influences of filling ratio, heat transfer rate, heat leakage position and tank size on the pressurization rate were analyzed. The results showed that the pressurization rate was mainly affected by the heat leakage position. His further study conducted in microgravity conditions indicated that the pressurization rate was lower than that in terrestrial gravity conditions due to the increase of wet-wall area and the enhancement of vaporization. Hasan et al. (1991) experimentally studied the thermal stratification and self-pressurization in LH2 storage tanks in terrestrial gravity conditions. Their results showed that with the increase of heat flux, the pressurization rate increased and the thermal stratification became severer. Lin et al. (1991) theoretically analyzed the performance of pressurization control devices, such as liquid jet mixing, passive insulation system and active cryogenic system in microgravity conditions. Using homogeneous thermodynamic model, they predicted that passive insulation system and active cryogenic system were suitable for long-term storage. Intermittent jet mixing and continuous jet mixing are only suitable for short-term storage, between them the former one is more effective. Lin and Hasan (1992) theoretically studied the thermal stratification and self-pressurization in a spherical LH2 storage tank in microgravity conditions. Using a simplified one-dimensional model with certain assumptions, such as uniform temperature in ullage, compressible and motionless liquid, effects of tank size, they studied the influences of liquid filling level and wall heat flux on the thermal stratification and self-pressurization. They claimed that the thermal expansion of liquid causes the condensation of vapor, and the wall heat flux leads to the evaporation of liquid at the interface. The combined effects of liquid filling level and wall heat flux determine the direction of mass transfer at the interface.

With the development of Computational Fluid Dynamics (CFD) and computation capacity, more accurate and sophisticated numerical studies on the phenomena of thermal stratification and self-pressurization in propellant storage tanks become a research hotspot. Hochstein et al. (1986) studied the pressurization control with SOLA-ECLIPSE software, and verified their results against the experimental results observed by Aydelott (1967a, 1967b) on the subject of influence of heating mode, tank size and gravity level, respectively. Later, they (Hochstein et al. 1990) conducted CFD studies on the influence of supercooling on the pressurization rate in full-size on-orbit storage tanks, the results showed that even a small amount of supercooling could significantly reduce the self-pressurization rate. Grayson et al. (2007) numerically studied self-pressurization through external heating and decompression through thermodynamic exhaust in gravity conditions. It is assumed that the liquid phase is incompressible and its density is only a function of temperature. The corresponding pressure and temperature predictions were in good agreement with the experimental results given by sensor measurements. Barsi and Kassemi (2008) proposed a two-phase CFD model to describe the self-pressurization behavior in a partially filled LH2 storage tank in normal gravity conditions. The predictive ability of the model was verified by experiments for different filling levels. Wang et al. (2013a, b) numerically investigated the pressurized discharge process in LH2 storage tank. Low Reynolds number *k*-epsilon model was adopted to deal with the heat exchange between fluid and wall. The gas amount required for pressurization, the thermal distribution and pressure change in the tank were studied in detail. They pointed out that the gas–liquid phase change had small effect on the pressurization behavior. Later Wang et al. (2013a, b) further conducted numerical simulations on the transient thermal state and pressurization behavior during discharge process. Both the heat exchange in tank and the external aerodynamic heating were studied with the foam insulation inside the computational domain taken into consideration.

Cryogenic Fluid Management (CFM) is one of the most important subjects in space engineering development. CFM involves several aspects such as Space Propellant Tank Supercharging Technology, On-Orbit Refueling Technology, Propellant Mass Measurement Technology, Thermodynamic Vent System (TVS) and Zero Boil-Off Technology (ZBOT). TVS and ZBOT mainly focus on propellant storage in space environment. LH2 as the propellant is easy to vaporize, which increases the pressure inside the tank and threatens the structural safety of the system. TVS can effectively reduce the internal pressure storage tank, however, it induces the waste of propellant to some extent. Moreover, exhausted gas distribution around the spacecraft brings potential risks to the spacecraft safety. Hastings et al. (2001) summarized the passive insulation technology that aims to reduce the external heat leakage using adiabatic insulation materials, but this technology cannot completely suppress the temperature stratification because of the very low boiling point of LH2. Besides, for the long-term on-orbit operations, passive insulation facilities increase the mass of tank and reduce spacecraft flexibility. At the end of last century, researchers from NASA proposed ZBOT to manage the long-term spacecraft propellant in the Mar's exploration project. They integrated the passive insulation technology and active refrigeration technology to realize the lossless storage of cryogenic propellant. There are two main types of active refrigeration technology, the first one is to export heat from inside of the tank to the outside by heat conduction device, and the second one is to reinforce the

fluid convection in the tank by mechanical agitation or cryogenic jet. The realization of the mechanical agitation is more complex, while the functional scope of the heat conduction devices is relatively narrow. In contrast, the pressure control by applying cryogenic jet inside storage tank seems more feasible and attractive.

Kassemi et al. (2017) evaluated the performance of the mass transfer and phase change models in calculating the pressurization in a cryogenic storage tank for three computational occasions. Ma et al. (2017) used CFD method to establish a model for studying the filling performance of hydrogen storage tank without exhaust liquid under microgravity conditions. In this model, both solid and fluid regions were considered to predict coupled heat transfer process. The effects of phase change during the filling process were also considered, and the mass and heat transfer models were embedded into CFD software FLUENT. Ma et al. (2018) adopted CFD method to simulate the depressurization process of a liquid hydrogen tank by using cryogenic fluid injection under microgravity conditions, the influences of the injection area, injection flow and injection velocity on the temperature field distribution and pressure variation in the tank were analyzed. They claimed that the depressurization performance of gas–liquid zone injection was better than that of single zone injection, and the depressurization effect of liquid zone injection was the weakest. Zuo et al. (2019) established a three-dimensional model of liquid hydrogen storage tanks with rotating nozzle, and studied the influence of cryogenic jet on thermal stratification under zero gravity by using CFD method. The results show that the rotating nozzle can effectively suppress the thermal stratification inside the tank. Guo et al. (2020, 2021) numerically studied the influence of nozzle shape, nozzle position and jet velocity on the effectiveness of cryogenic jet for eliminating the thermal stratification by using a two-dimensional model storage tank, and the result showed that the elimination effect of circular jet nozzle was better than that of hemispherical jet nozzle.

Although efforts have been made to solve this problem and some progress has been accomplished, most of the previous studies assumed a uniform temperature distribution inside the tank at the beginning of numerical simulation. The boundary heat leakage and cryogenic jet flow were carried out simultaneously in the simulation. However, the tank body is generally made of metal material and covered with multilayer of thermal insulation material, such that the heat penetration cannot be completely eliminated. Generally, the heat penetrated into the liquid propellant through the tank wall is not uniformly distributed, and the heat leakage area greatly affects the thermal stratification inside the tank. Therefore, it is necessary to figure out the stratified temperature distribution and take it as the initial condition in practical numerical investigations.

In the present study, a CFD model is introduced to predict the time evolution of a process in which cryogenic jet injection is used to suppress the thermal stratification inside a liquid hydrogen storage tank. The numerical simulation was divided into two stages. In the first stage, a spherical ullage was located in the center of the tank, which is a typical liquid–gas distribution in a tank during long term on-orbit operation period under microgravity conditions (Li et al. 2020b). In order to quickly obtain the temperature distribution in the tank, we only consider the heat leakage occurring on the wall of tank, neglecting the effects of surface tension and phase change. In the second stage, we take both surface tension and phase change into account to investigate the complete physical problem, in which the thermal and phase distributions calculated in the first stage were treated as the initial condition in the study. Then, the suppression processes of temperature stratification by cryogenic jet injection were analyzed in detail for different mass flow rates and filling ratios.

CFD Modeling and Numerical Method

Physical Model

Here, we focus on the effect of a cryogenic jet injected into a partially filled large tank to eliminate the temperature stratification of propellant. A complete two-dimensional axisymmetric storage tank model was adopted for the numerical simulation. On top of the tank, a cryogenic jet nozzle with the radius of 55 mm was inserted into the tank. The specific dimensions of each part of the tank are shown in Fig. 1, in which the origin of the coordinates locates at the center of the tank.

Mathematical Model

The physical model is governed by continuity, momentum and energy equations which can be written as:

(1) Continuity equation

$$\frac{\partial \rho}{\partial t} + \nabla \cdot (\rho \boldsymbol{u}) = 0 \tag{1}$$

(2) Momentum equation

$$\frac{\partial}{\partial t}(\rho \boldsymbol{u}) + \nabla \cdot (\rho \boldsymbol{u}\boldsymbol{u}) = -\nabla p + \nabla \cdot \left[\mu_{\text{eff}}\left(\nabla \boldsymbol{u} + \nabla \boldsymbol{u}^T\right) - \frac{2}{3}\mu_{\text{eff}}(\nabla \cdot \boldsymbol{u})\boldsymbol{I}\right] + \rho \boldsymbol{g} + \boldsymbol{F}_M \tag{2}$$

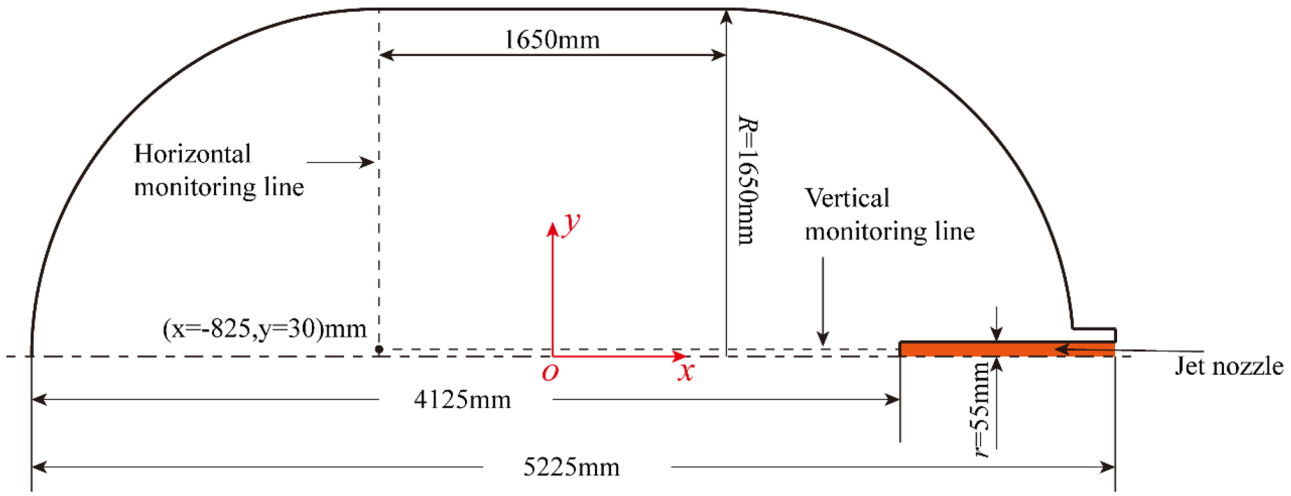

Fig. 1 Schematic diagram of propellant storage tank and monitor lines

(3) Energy equation

$$\frac{\partial}{\partial t}(\rho c_p T) + \nabla \cdot (\rho c_p T \boldsymbol{u}) = \nabla \cdot \left(\lambda_{\text{eff}} \nabla T\right) + S_h \tag{3}$$

Here the density $\rho = \alpha_l \rho_l + (1-\alpha_l)\rho_g$, α is the volume fraction satisfying $\alpha_l + \alpha_g = 1$, the subscript l and g stands for the liquid and gas phases. The effective viscosity $\mu_{\text{eff}} = \mu + \mu_t$, where $\mu = \alpha_l \mu_l + (1-\alpha_l)\mu_g$, and μ_t is the turbulent viscosity defined in later. The $\boldsymbol{I}$ is the unit second order tensor. The c_p is the specific heat at constant pressure. The thermal conductivity $\lambda = \alpha_l \lambda_l + (1-\alpha_l)\lambda_g$, and the effective thermal conductivity $\lambda_{\text{eff}} = \lambda + \lambda_t = \lambda + c_p \mu_t / \text{Pr}_t$, where the turbulent Prandtl number $\text{Pr}_t \approx 0.85$ in present study. The S_h is source term which will be defined later.

(4) Turbulent model.

The flow in the tank is assumed nearly turbulent. The low Reynolds (Re) k-epsilon (k-ε) model is adopted to acquire more adequate numerical results. The governing equations of k-ε model are given by

$$\frac{\partial}{\partial t}(\rho k) + \nabla \cdot (\rho k \boldsymbol{u}) = \nabla \cdot \left[\left(\mu + \frac{\mu_t}{\sigma_k}\right)\nabla k\right] + G_k - \rho\varepsilon - D_k \tag{4}$$

$$\frac{\partial}{\partial t}(\rho \varepsilon) + \nabla \cdot (\rho \varepsilon u) = \nabla \cdot \left[\left(\mu + f_\mu \frac{\mu_t}{\sigma_\varepsilon}\right)\nabla \varepsilon\right] + C_1 f_1 \frac{\varepsilon}{k} G_k - C_1 f_2 \rho \frac{\varepsilon^2}{k} \tag{5}$$

where the turbulent viscosity $\mu_t = \rho C_\mu \frac{k^2}{\varepsilon}$. The source term

$$G_k = f_\mu \mu_t \nabla \boldsymbol{u}\left(\nabla \boldsymbol{u} + \nabla \boldsymbol{u}^T\right), D_k = 2\mu\left(\frac{\partial k^{1/2}}{\partial n}\right)^2$$

The constants and coefficients in above equations are as follows:

$$f_1 = 1.0, f_2 = 1.0 - 0.3\exp\left(-\text{Re}_t^2\right), f_\mu = \exp\left(-\frac{2.5}{1 + \text{Re}_t/50}\right),$$

where $\text{Re}_t = \frac{\rho k^2}{\varepsilon \mu}$, and.

$C_\mu = 0.09,\quad C_1 = 1.44,\quad C_2 = 1.92,\quad \sigma_k = 1.0,\quad \sigma_\varepsilon = 1.3.$

(5) Multiphase model.

In present study, the Volume of Fluid (VOF) method was adopted to capture the two-phase flow in the tank, which has been validated in the work of Li et al. (2018, 2020a). The governing equation of VOF is given by

$$\frac{\partial}{\partial t}\left(\alpha_l \rho_l\right) + \nabla \cdot \left(\alpha_l \rho_l \boldsymbol{u}_l\right) = S_m \tag{6}$$

where S_m is the mass source term defined in the phase change model.

The source term F_M in the momentum Eq. (2) stands for the effect of surface tension coming from the liquid–gas interface. Here we adopt the continuum surface force (CSF) model (Brackbill et al. 1992), which is given by

$$\boldsymbol{F}_M = \sigma \frac{\rho \kappa_g \nabla \alpha_g}{\frac{1}{2}\left(\rho_g + \rho_l\right)} \tag{7}$$

where σ is the surface tension coefficient. The curvature $\kappa = -\nabla \cdot \hat{n}$, and the normal vector $\hat{n} = \frac{\nabla \alpha}{\|\nabla \alpha\|}$.

(6) Phase change model.

Here, we adopt the broadly used phase change model proposed by Lee (1979) to the VOF Eq. (6) as a source term S_m which is given by

Table 1 Settings of CFD model

Project	Detailed Settings
Computational model	Low Re k-ε Model
	Continuous Surface Force model (CFS) (Brackbill et al. 1992)
	VOF multiphase flow model
	Evaporation and condensation model (Lee model) (Lee 1979)
Boundary conditions	Constant heat flux boundary condition on tank wall: 1 W/m^2
	Inlet: mass-flow inlet, T_{in} = 18 K
	Outlet: mass-flow outlet, T_{out} = 20 K
Calculation method	Pressure velocity coupling: PISO
	Gradient: Least Squares Cell Based method
	Pressure: PRESTO
	Interface: Geo-Reconstruct
	Momentum and energy discretization: Second Order Upwind
Initial conditions	Initial pressure: 90,717 Pa
	Initial temperature: 20 K
Time steps	0.00001 s—0.01 s

$$S_m = \begin{cases} C\alpha_l\rho_l\frac{(T_l - T_{sat})}{T_{sat}} & T_l > T_{sat}, \text{evaporation} \\ C\alpha_g\rho_g\frac{(T_{sat} - T_g)}{T_{sat}} & T_v < T_{sat}, \text{condensation} \end{cases} \quad (8)$$

where C is the relaxation time coefficient with the unit of s^{-1}, whose value is set as 0.1 (Schepper et al. 2009). T_{sat} is the saturation temperature. Then the heat source S_h in the energy Eq. (3) can be calculated by

$$S_h = S_m \cdot \Delta h \quad (9)$$

where Δh is the latent heat, J/kg.

Numerical Method

The software ICEM was used to generate unstructured grid which was refined near the wall. The solution of the governing equation was obtained via FLUENT 17.2, a widely used CFD simulation software. The phase change model and source terms were implemented by User Defined Function (UDF). The detailed settings of the computational model, boundary conditions, computational discrete method and initial conditions are depicted in Table 1. In the whole computation process, it was assumed that the gas phase is ideal gas and the liquid phase satisfied the Boussinesq assumption of $\rho_l = \rho_{l0}[1 - \beta(T - T_0)]$, where the density ρ_{l0} is 71.26 kg/m^3 at the initial temperature of 20 K, and the volume expansion coefficient β is 0.018 K^{-1}. The other physical parameters of the working medium were set as the function of temperature, and their values at the initial temperature 20 K are shown in Table 2. The influences of the cryogenic jet conditions on the evolution of fluid flow and temperature distribution were studied by changing the mass flow rate and initial filling ratio of the cryogenic jet.

Grid Independence

In this study, the grid independence test was carried out by using three different grid numbers 21045 (Grid1), 41,310 (Grid2), and 74,994 (Grid3). The horizontal and vertical monitoring lines in Fig. 1 were selected at the positions with large temperature gradient in the computational domain. Figure 2 shows the temperature distributions at the vertical and horizontal monitoring line, for the case of tank filling ratio of 87% and mass flow rate of 0.14 kg/s after 4.28 s cryogenic jet injection. As can be seen from Fig. 2a, the temperature distribution along the vertical monitoring line is nearly the same for three different grids. In Fig. 2b, tiny temperature distribution differences can be found along the horizontal monitoring line in both the relatively fine Grid2 and Grid3, but their trend is the same, and the influence of grid number is negligible. Near the jet nozzle location, the rough Grid1 is difficult to capture the details of the temperature distribution curve. Therefore, the grid number 41310 (Grid2) was adopted in the subsequent simulations considering both accuracy and cost of the computation.

Results and Discussion

In the present study, the numerical simulation was carried out under designed conditions (see Table 3) to study the influence of the incident mass flow rate with different filling ratios on the internal temperature stratification of the tank and on

Table 2 Thermal physical property values of liquid hydrogen at 20 K

Parameters	μ (Pa•s)	c_p (J/(kg•K))	λ (W/(m•K))
Value	1.37×10^{-5}	9.56×10^{3}	0.10329

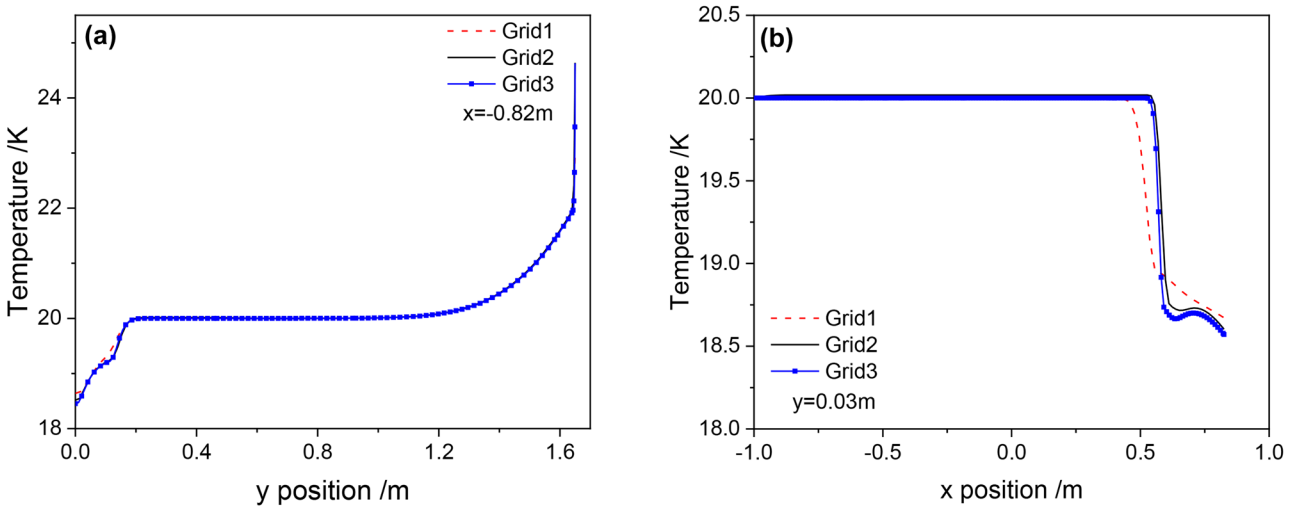

Fig. 2 Grid independence test. (**a**) Temperature distribution at the vertical monitoring line; (**b**) Temperature distribution at the horizontal monitoring line.

the position and shape of the ullage. Firstly, the influences of incident mass flow rate on the fluid temperature stratification, pressure variation and mass transfer in the storage tank were investigated for different filling ratios. Then, the effects of filling ratio on the same physical quantities as in the first part were studied and analyzed for different incident mass flow rates.

Influence of Incident Mass Flow Rate

Here, the influence of incident mass flow rate on the elimination of temperature stratification and the change of ullage in the tank was studied for three typical filling ratios of 98%, 87% and 78%. The numerical simulation was divided into two stage. In the first stage, a spherical ullage was located at the center of the tank, which is a typical liquid–gas distribution in a tank during long term on-orbit operation under microgravity condition (Li et al. 2020b). In order to quickly obtain the temperature distribution in the tank, we only considered the heat leakage occurring on the wall of tank, neglecting the effects of surface tension and phase change. In the second stage, we take both of the surface tension and phase change into account to investigate the influence of cryogenic jet injection on the thermal stratification in the storage tank, in which the thermal and phase distributions calculated in the first stage were taken as the initial condition.

Table 3 Details of the numerical simulation cases

Case	Radius of bubble R (mm)	Filling ratio (%)	Incident mass flow rate (kg/s)
1	500	98	0.035
2	500	98	0.070
3	500	98	0.140
4	1000	87	0.035
5	1000	87	0.070
6	1000	87	0.140
7	1200	78	0.035
8	1200	78	0.070
9	1200	78	0.140

(1) Filling ratio of 98%

The radius of the ullage bubble is 500 mm for the liquid filling ratio of 98% in the storage tank. As mentioned in the numerical simulation method, the phase and temperature distribution after 10 days of heat leakage in the first stage are calculated and shown in Fig. 3, in which the original position of the ullage was marked with yellow line in the phase distribution panel. It can be seen from Fig. 3 that the thermal stratification distributed from the wall of tank to the center, and the ullage (red area in the left phase contour) stays at the center of the tank steadily.

The contours of the phase and temperature distribution changing with cryogenic jet injection time are shown in Fig. 4 for the incident mass flow rate of 0.035 kg/s. It can be seen that as the jet injection lasts for 60 s, the cryogenic fluid arrives at the gas–liquid interface and causes a weak deformation of the interface. At this moment, change of the contours of the temperature distribution is not distinct, but the cryogenic liquid near the jet nozzle has formed a cryogenic fluid column. With the passage of injection time, the injection fluid continually squeezes the bubble. When the jet flow lasts for 160 s, the ullage (gas bubble) is impacted by the cryogenic jet, deformation of gas–liquid interface

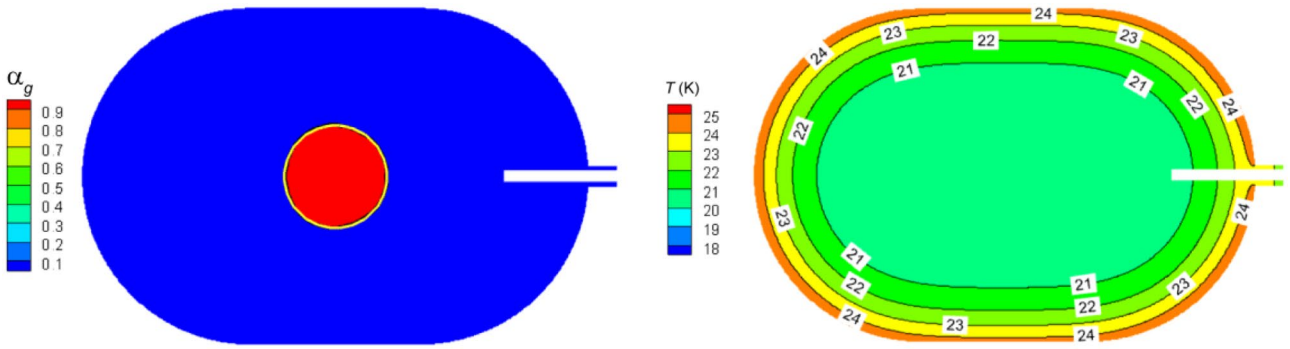

Fig. 3 Contours of the phase distribution (left) and static temperature distribution (right) at the initial time of jet flow for filling ratio of 98%

becomes more evident, and the ullage starts to move towards the bottom of the tank. It can be found from the contour of temperature that the cryogenic jet begins to envelop the ullage. As the cryogenic jet lasts for 260 s, the displacement of ullage along the axis of the storage tank is rather distinct. When the jet lasts for 390 s, it can be noted that the shape of ullage recovers slightly. Under the influence of cryogenic jet injection, the ullage exhibits dynamic behaviors both in its shape and its position in the tank. This is similar to the results found in the study on liquid sloshing by Li et al. (2020a). Moreover, it can be found that the cryogenic jet fluid is always on the top side of the ullage bubble.

Figure 5 shows the contours of the phase and temperature distribution changing with cryogenic jet injection time for the incident mass flow rate of 0.07 kg/s. It can be seen that when the jet lasts for 28 s, the cryogenic fluid has arrived at the gas–liquid interface and caused a deformation in the interface. Afterwards, the cryogenic jet continues to squeeze the ullage bubble. When the cryogenic jet lasts for 81 s, the deformation of the ullage bubble is rather distinct. The bubble is squeezed into a sunken shape, but its location doesn't change significantly. At this moment, there is a small change in the contour of temperature distribution, and the cryogenic fluid column continually advances along the central axis. Then, the cryogenic jet drives the ullage bubble toward the bottom of the tank. Around the time of 145 s, as shown in Fig. 5c, the position of the ullage bubble drifts away obviously. Because of gas–liquid interface deformation and heat leakage, tiny gas bubbles start to take form. In the axisymmetric model. This means that gas ring is formed around the central axis of the storage tank, which may be a deficiency in taking a two-dimensional axisymmetric model to simulate the three-dimensional interface. In subsequent discussions, we mainly focus on the shape and position of the large ullage bubble. When the cryogenic jet injection continues to 290 s, the ullage bubble is pushed and squeezed by the jet to a position near the bottom of the tank, and the sunken ullage originally caused by the jet squeezing gradually recovers to the shape of a ball. Meanwhile, the temperature near the cryogenic side decreases slightly.

Figure 6 shows the contours of the phase and temperature distribution changing with cryogenic jet injection time for the incident mass flow rate of 0.14 kg/s. It can be seen that when the jet lasts for 13 s, cryogenic fluid has already squeezed the gas–liquid interface. This time interval is much shorter as compared with those in the cases of mass flow rate of 0.035 kg/s and 0.07 kg/s. Thereafter, the cryogenic jet penetrates the ullage bubbles at the time of 31 s or so. It is noted that the location of bubble does not change significantly. Then, the bubbles driven by the cryogenic jet move continually toward the bottom of the tank, as shown in Fig. 6c at the time of 108 s. Similarly, tiny bubbles are generated in front of the cryogenic fluid. The large ullage bubble arrives at the bottom of the tank. The shape and position of the ullage change significantly as compared with its original state at the center of the tank. It can be seen from the contour of temperature that at this moment the jet column formed by the cryogenic fluid has run through the axis of the whole tank body, and a cryogenic area is formed near the axis. The thermal stratification at the bottom of the tank was completely destroyed. As the cryogenic jet lasts for 208 s, more gas phase mass is carried to the bottom of the tank, and the newly generated bubbles turn into separated. The distribution of the gas and liquid phase becomes more irregular.

With the three cases for different incident mass flow rates taken together, it can be seen that, for a given filling ratio, a small incident mass flow rate can only cause a displacement of the ullage region, and a very large incident mass flow rate is required to penetrate the ullage region. In order to quantitatively analyze the influence of incident mass flow rate on the evolutions of temperature and two-phase flow field in a tank, the volume averaged variables

$$\bar{f} = \frac{1}{V}\int_V f \mathrm{d}V \tag{10}$$

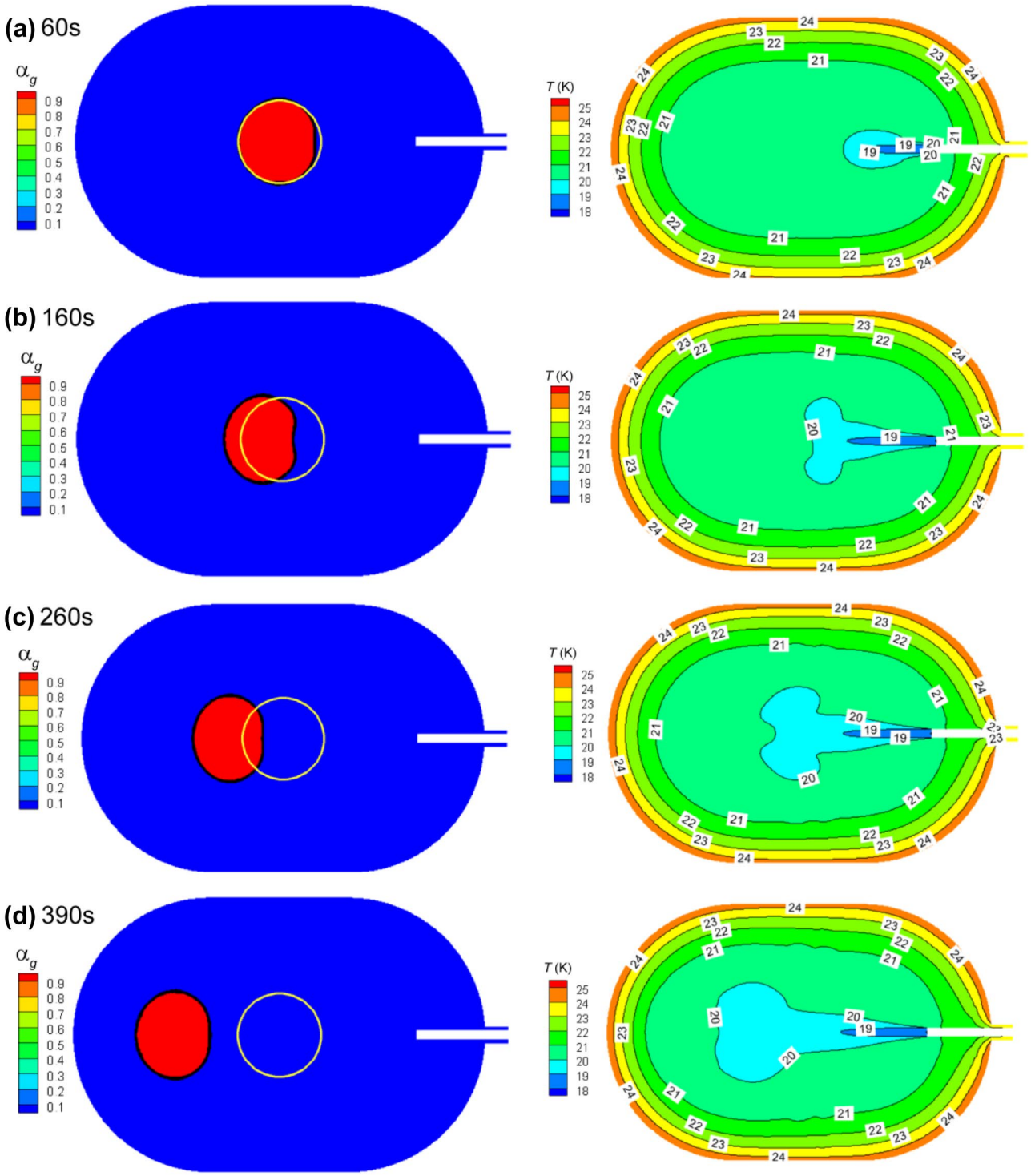

Fig. 4 Time evolution of contours of phase and temperature distribution for case 1

for the temperature, pressure and velocity in the tank are selected, where f stands for the local variables to be averaged. Meanwhile, the integrated mass of evaporation is given by

$$M = \int_t \int_V S_m \mathrm{d}V\mathrm{d}t \tag{11}$$

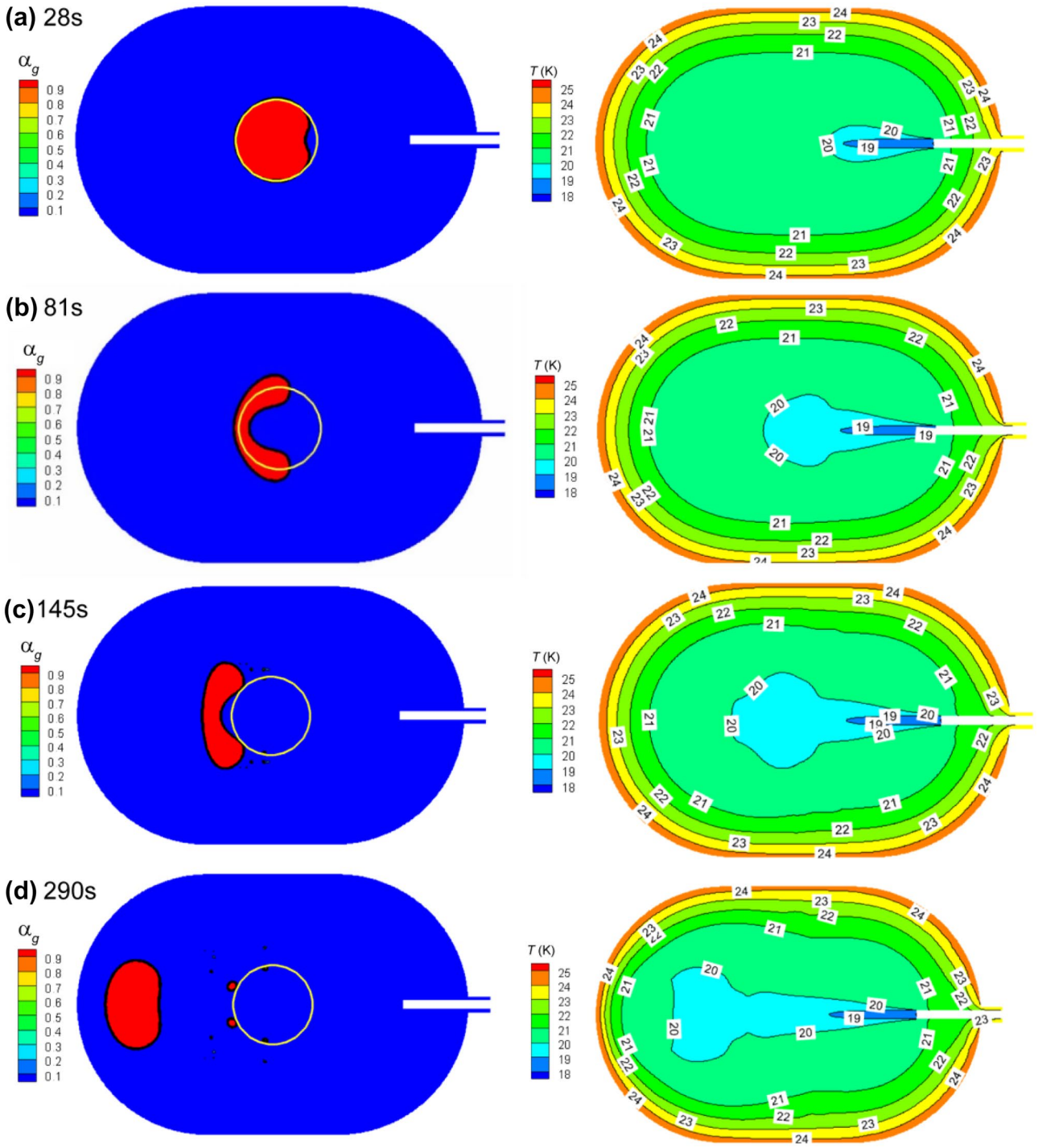

Fig. 5 Time evolution of contours of phase and temperature distribution for case 2

where S_m is defined by Eq. (8) in the phase change model. In Fig. 7, we depict the relations between the above selected variables and the incident fluid mass which equals the flow rate times injection time.

It can be seen from Fig. 7a that the average temperature of the storage tank continually decreases during the injection process. For the same incident fluid mass, the larger the incident mass flow rate, the sharper the decrease. In Fig. 7b, when the incident fluid mass is less than 7 kg, for the same incident fluid mass, the lager the incident mass flow rate, the lower the average pressure in the tank. However, after this point (7 kg), the average pressure for the mass flow rate of

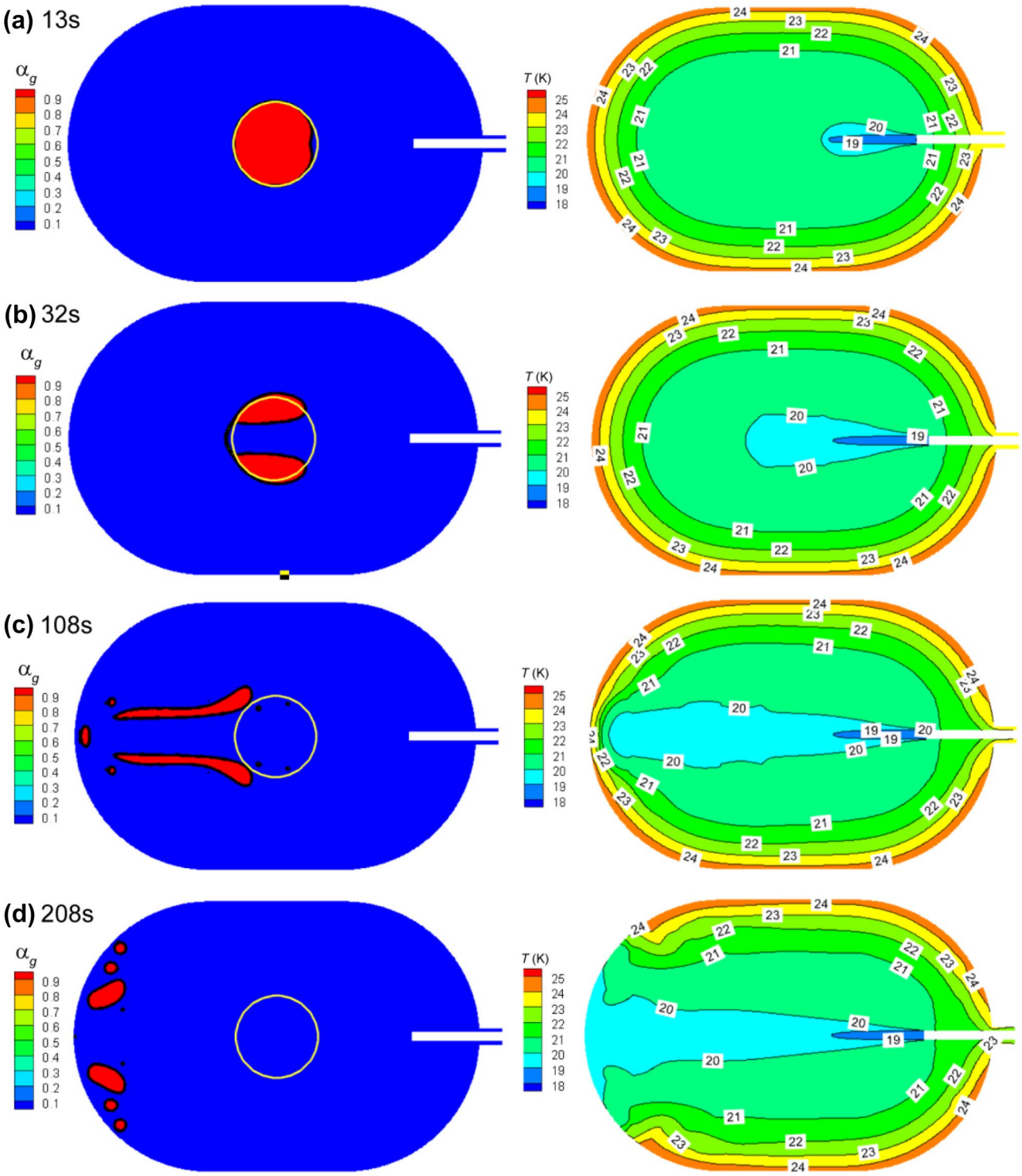

Fig. 6 Time evolution of contours of phase and temperature distribution for case 3

0.035 kg/s (case 1) declines to lower than that in the other two cases, and eventually increases when the incident fluid mass is larger than 12 kg. This is because the high mass flow rate jet pushes the ullage zone to the high temperature area near the wall, resulting in intensification of evaporation, and correspondingly leading to a faster increase of pressure. By contrast, condensation (i.e. when the value of evaporation is negative) occurs in the decrease part of pressure for the low mass flow rate cases, as can be seen in Fig. 7d. In the cryogenic jet injection process, higher inlet jet velocity

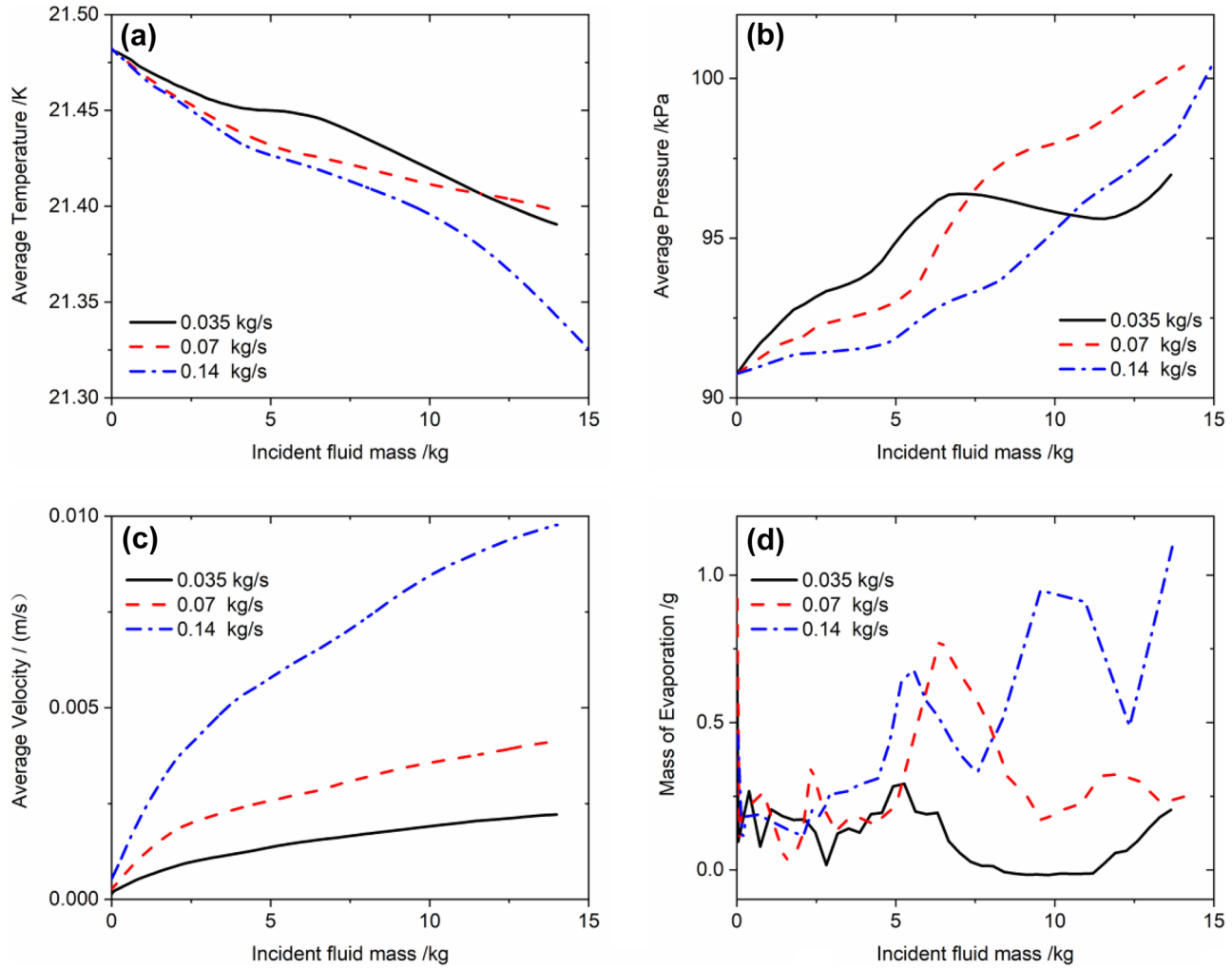

Fig. 7 Physical properties averaged over the tank versus incident fluid mass for 98% filling ratio

results from larger mass flow rate for the same designed structure. Correspondingly, the average velocity in the tank exhibits the same trends, as shown in Fig. 7c. Figure 7d shows the change of evaporation with increasing incident fluid mass. It can be found that the mass of evaporation in the tank fluctuates with the increase of incident fluid mass. Basically, the higher the incident mass flow rate, the heavier the evaporation. However, the magnitude of the evaporation mass is very small. On one hand, the quantity of evaporation is decided by the position of the ullage, i.e. the temperature distribution around the gas–liquid interface. On the other hand, the cryogenic jet affects where the ullage goes. The physical variables are collectively determined by these two factors. The high incident mass flow rate jet destroys the thermal stratification and produces obvious flow of the fluid in the tank. And thus the cryogenic jet has a significant effect on the reduction of the temperature.

(2) Filling ratio of 87%

The radius of the ullage bubble is 1000 mm for the liquid filling ratio of 87% in the storage tank. The phase and temperature distribution after 10 days of heat leakage in the first stage are calculated, as shown in Fig. 3, in which the thermal stratification distributed from the wall of tank into the center, and the ullage stays in the center of the tank steadily. As compared with case 1 (98% filling ratio), the temperature distribution exhibits small difference near the center of the wall where the distance between the wall and the gas–liquid interface is the smallest. Obviously, closer distance causes faster heat conduction due to the larger thermal diffusivity of the gas phase (see Fig. 8).

The contours of the phase and temperature distribution changing with cryogenic jet injection time are shown in Fig. 9 for the incident mass flow rate of 0.035 kg/s. It can be

seen that the cryogenic jet fluid reaches the region of ullage and causes a faint deformation of the gas–liquid interface when the jet injection lasts for about 23 s. With the passage of time, the injected cryogenic fluid continually squeezes the bubble. When the jet lasts more than 103 s, the ullage deformation due to the impact of the cryogenic jet becomes more evident. By observing the contour of the temperature distribution in the tank at this moment, it is found that the temperature rise in the ullage region is higher than that in the adjacent liquid region. When it comes to the time moment of 253 s, the ullage slightly moves towards the bottom of the tank, accompanied with a further increase of temperature inside. Besides, the injected cryogenic fluid gathers at the top of the tank due to the block effect of the relatively large ullage zone. When the jet lasts for 393 s, obvious deformation and deviation of the ullage from its original state can be found. And little bubbles are still produced just as in case 1. Notably, local high temperature region is generated inside the bubbles. On one hand, this is attributed to the heat transfer from the wall in view of the relatively shorter distance between the ullage and the wall. On the other hand, the increased pressure in the ullage region leads to the rising of temperature in accordance with the Clapeyron's equation of ideal gas, $pV = nRT$.

Figure 10 shows the contours of the phase and temperature distribution changing with cryogenic jet injection time for the incident mass flow rate of 0.07 kg/s. It can be seen that when the cryogenic jet lasts for about 14 s, the cryogenic fluid has arrived at the ullage region and causes a deformation of the gas–liquid interface. In this stage the change of temperature is not distinct, except for the ullage region where there is a little stronger heat transfer. Afterwards, the cryogenic jet begins to continually squeeze the ullage bubble until the time of about 84 s when the injection fluid penetrated into the bubble, while the location of the bubbles remains nearly unchanged. The temperature along the axis of the tank decreases due to the running through of the cryogenic jet fluid, despite the rising of temperature in the penetrated bubbles. At about 214 s, small bubbles are created by cryogenic jet flow and the jet reaches the bottom of the tank. The cryogenic fluid column runs through the entire tank axis, forming a cryogenic area around the central axis of the tank. When cryogenic jet continues to about 294 s, the bubbles at the bottom of the tank become larger, while resting still at the bottom of the tank. Nevertheless, the main ullage region is still located nearly at the center of the tank, rather than driven towards the bottom of the tank as in case 2. Therefore, there are new thermal stratification region generated around the ullage region where the temperature is high.

Figure 11 shows the contours of the phase and temperature distribution changing with cryogenic jet injection time for the incident mass flow rate of 0.14 kg/s. It is found that when the jet lasts for 13 s, the cryogenic fluid has severely squeezed the gas–liquid interface and the jet reaches the center of the ullage bubble with its position relative to the tank remained unchanged. As the jet injection continues, the cryogenic fluid penetrates through the ullage bubbles at the time of 33 s or so, and new tiny bubbles are also generated in front of the cryogenic fluid. At this moment, there is no high temperature region inside the penetrated bubble. The small bubbles, as well as the ullage bubble continually move towards the bottom of the tank due to the driving action of the cryogenic jet, as shown in Fig. 11c. At the time about 193 s, more gas phase is carried to the bottom of the tank by the jet flow. Similar to the case of mass flow rate of 0.07 kg/s (case 5), the ullage region staying in the center of the tank exhibits high temperature.

From the above case study for filling ratio of 87%, it is found that a jet with relatively large mass flow rate can penetrate the ullage bubble while the position of ullage remains nearly unchanged. With the passage of time, there is an increase of temperature in the ullage bubble, while the ullage position stays in the center of the tank. In order to quantitatively analyze the influence of incident mass flow rate on the evolution of temperature and two-phase flow field,

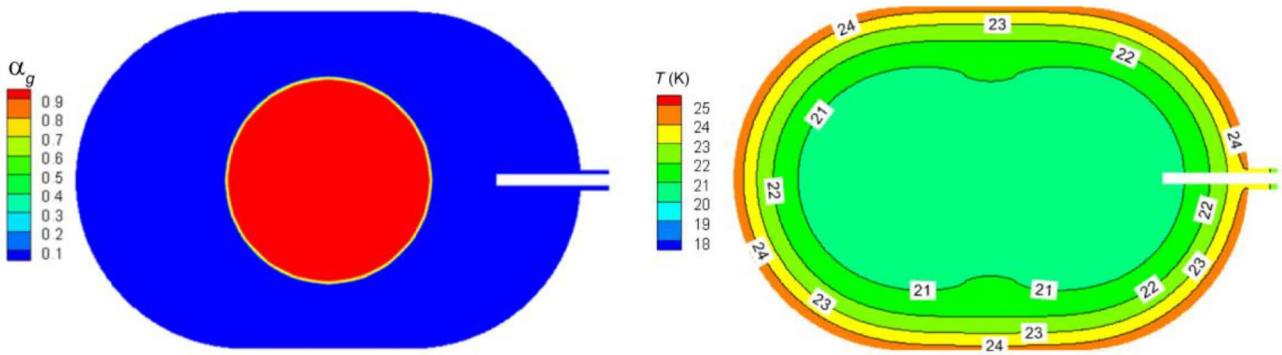

Fig. 8 Contours of the phase distribution (left) and static temperature distribution (right) at the initial time of jet flow for filling ratio of 87%

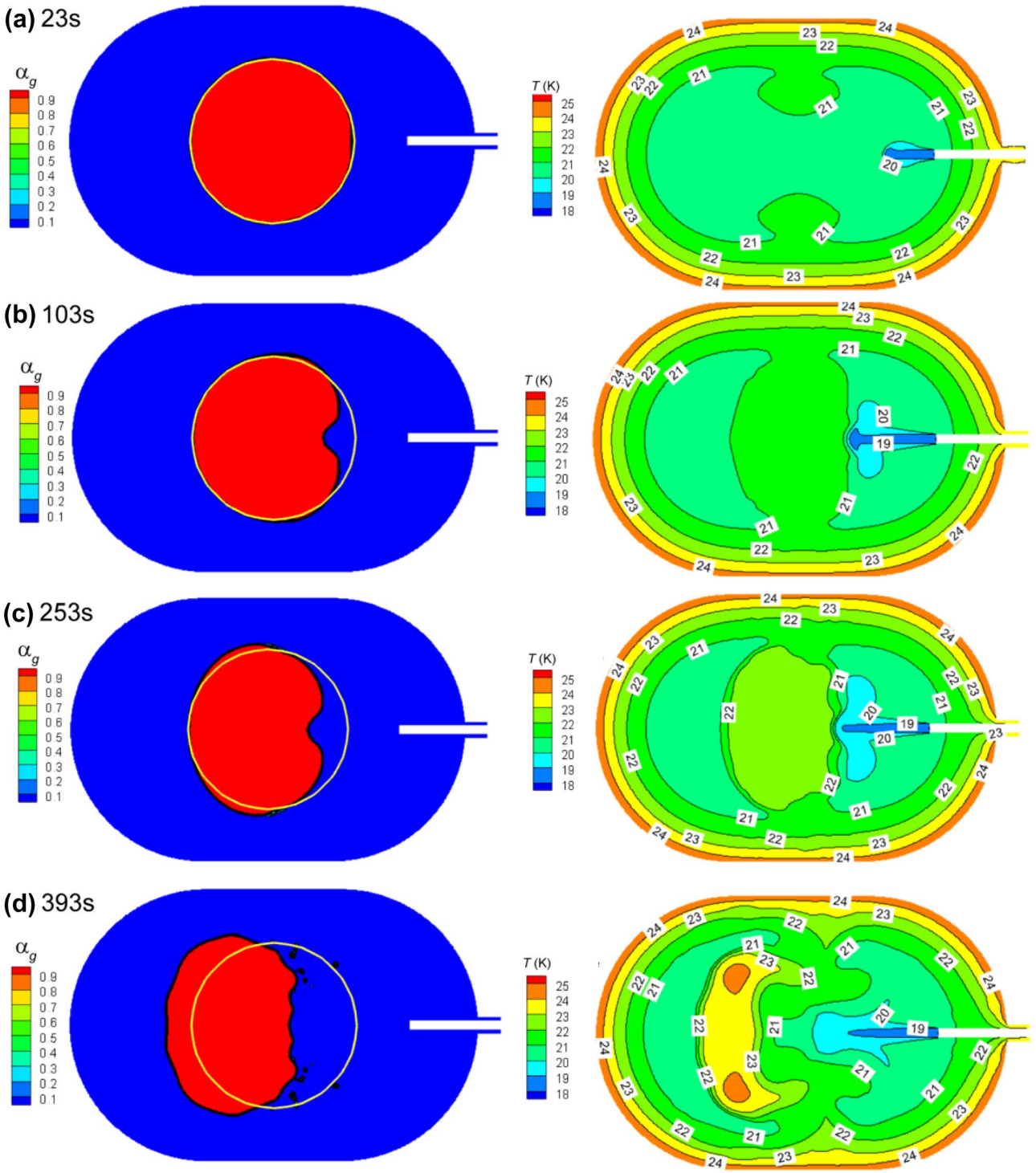

Fig. 9 Time evolution of contours of phase and temperature distribution for case 4

the relations between the temperature, pressure, velocity, mass of evaporation and the incident flow mass are shown in Fig. 12.

As is shown in Fig. 12a, the average temperature decreases slightly with increasing incident fluid mass, excepting for the case of small mass flow rate of 0.035 kg/s, in which the cryogenic jet flow cannot penetrate through the ullage bubble. For the same incident fluid mass, higher incident mass flow rate results in lower average temperature in the tank, which is related to the fact that high incident

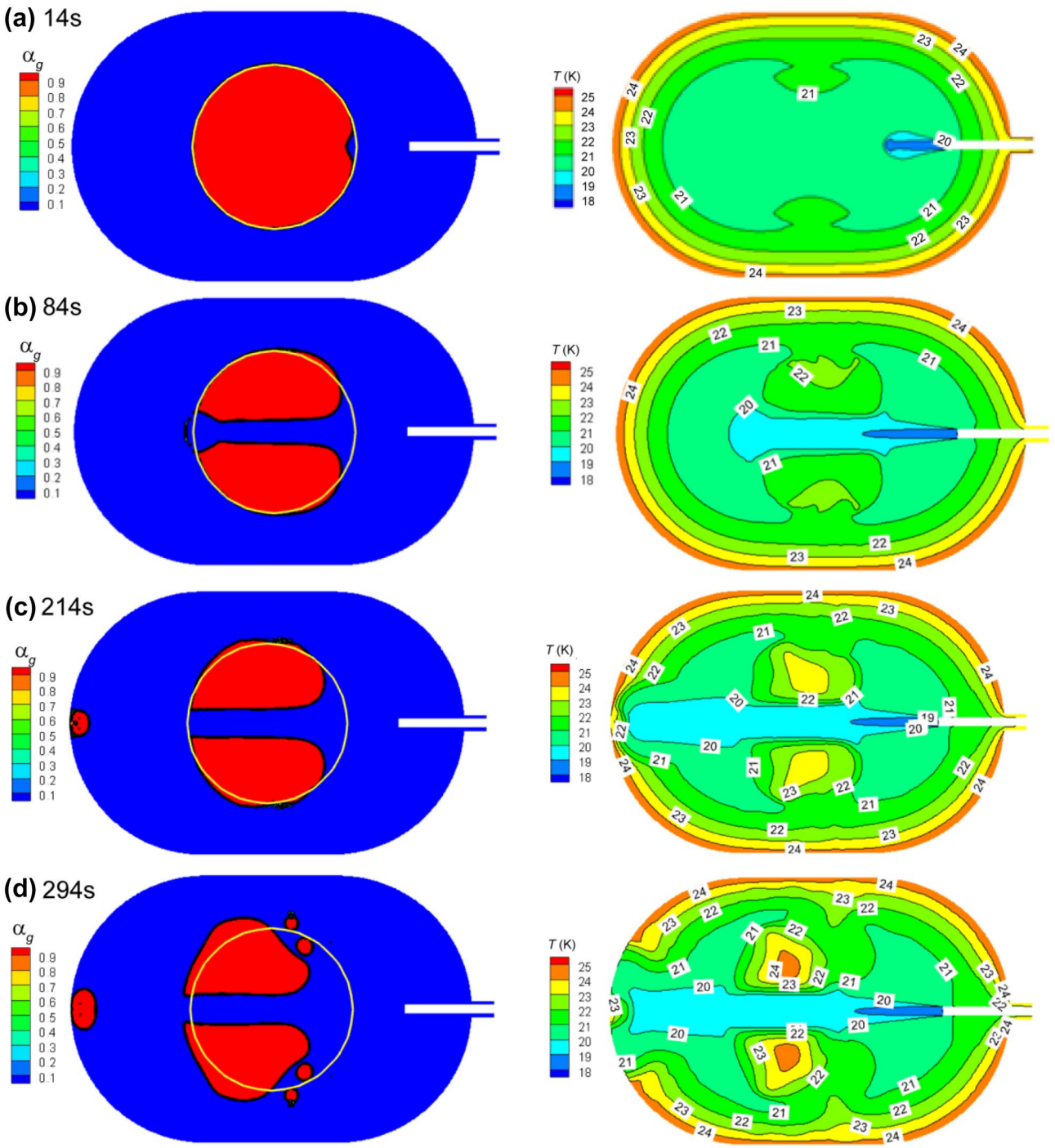

Fig. 10 Time evolution of contours of phase and temperature distribution for case 5

mass flow rate can quickly deform the gas phase distribution inside the tank and promotes convection and mixture process of the hot and the cold liquids. The average velocity of convection in the tank is shown in Fig. 12c, from which we can found that the average velocity increases with increasing incident mass flow rate, and higher mass flow rate leads to larger average velocity. As for the average pressure in the tank shown in Fig. 12b, it can be seen that larger incident mass flow rate is more efficient to reduce the pressurization, though there is an increasing trend of the average temperature for all the three cases with different mass flow rates. Figure 12d shows the relationship between evaporation and incident fluid mass. It can be found that at the beginning of the cryogenic jet injection, the evaporation

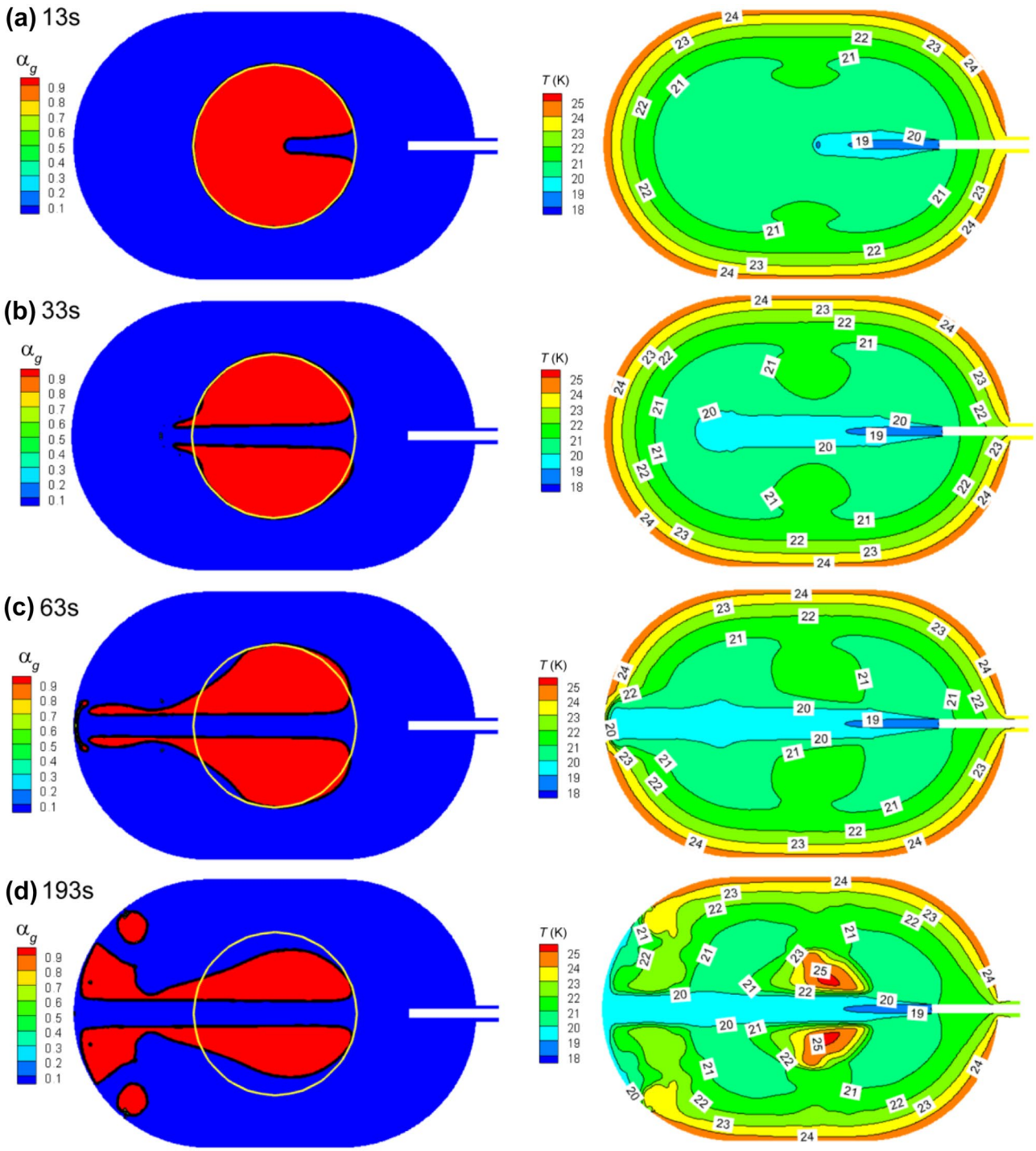

Fig. 11 Time evolution of contours of phase and temperature distribution for case 6

in the tank is effectively suppressed. With the increase of the incident fluid mass, the mass of evaporation in the tank fluctuates. As in the aforementioned analysis for the filling ration of 98%, the high incident mass flow rate destroys temperature stratification, promotes the fluid flow and effectively reduces the evaporation in the tank.

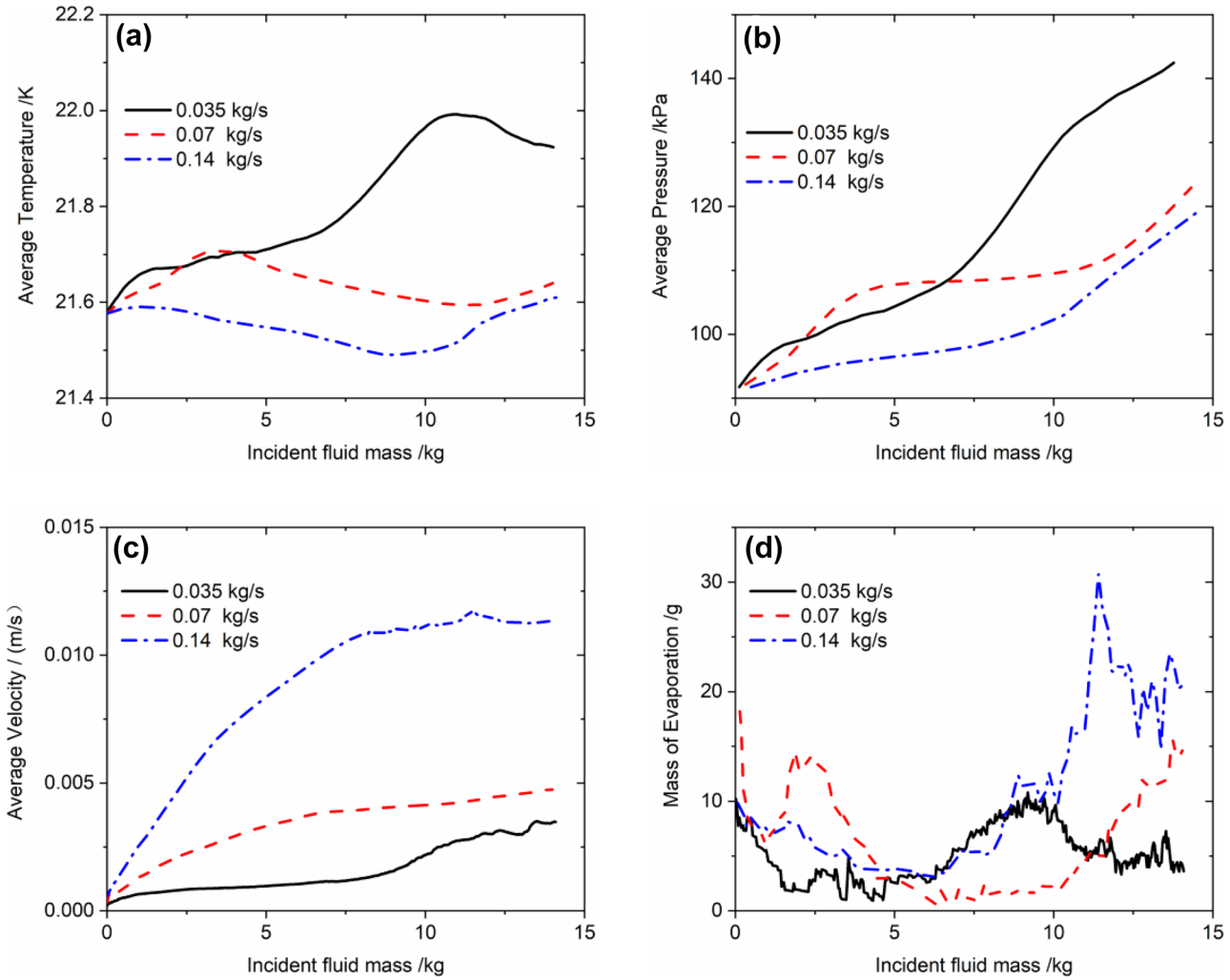

Fig. 12 Physical properties averaged over the tank versus incident fluid mass at 87% filling ratio

(3) Filling ratio of 78%

The radius of the ullage bubble is 1200 mm for the liquid filling ratio of 78% in the storage tank. The phase and temperature distribution after 10 days of heat leakage in the first stage are calculated, as shown in Fig. 13, in which the thermal stratification distributed from the wall of tank to the center, and the ullage stays at the center of the tank steadily.

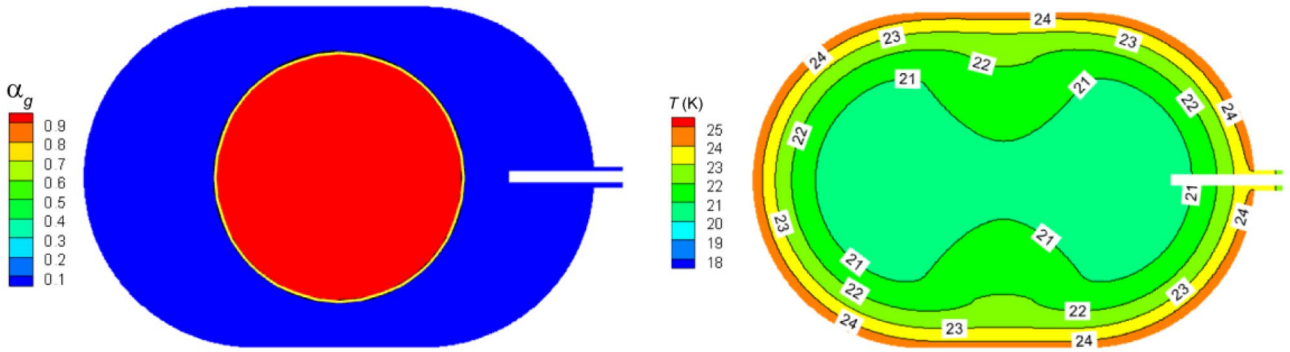

Fig. 13 Contours of the phase distribution (left) and static temperature distribution (right) at the initial time of jet flow for filling ratio of 78%

As compared with the cases of 98% and 87% filling ratio, there is a more fierce heat transfer near the center of the wall where the distance between the wall and the gas–liquid interface is the smallest.

Figure 14 shows the contours of the phase and temperature distribution changing with cryogenic jet injection time for a given incident mass flow rate of 0.035 kg/s. As compared with the larger filling ratio of 98% and 87%, the

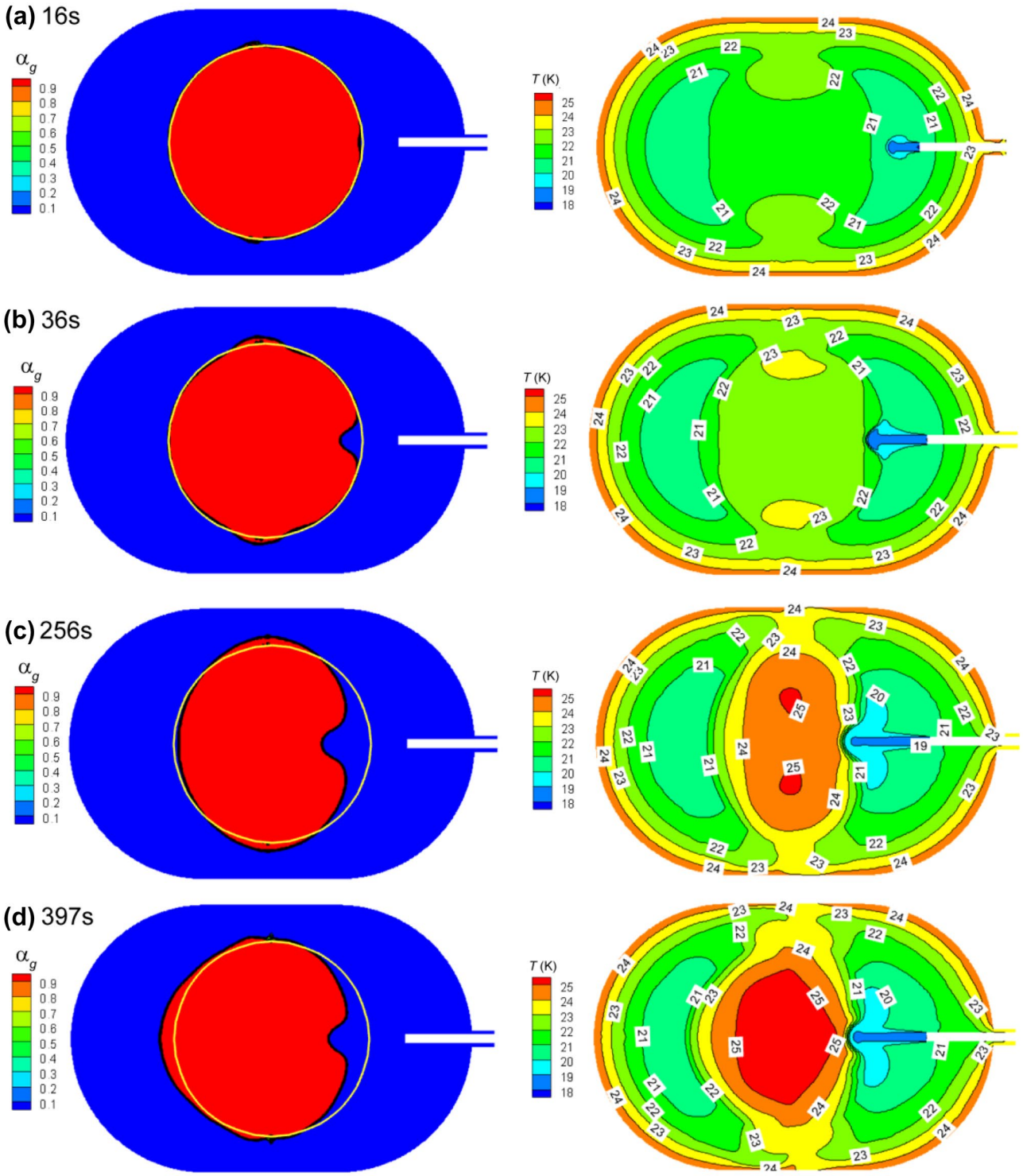

Fig. 14 Time evolution of contours of phase and temperature distribution for case 7

cryogenic jet fluid arrives at the gas–liquid interface in a shorter time period of 16 s or so. The interface exhibits slight deformation with a little pit on top of the ullage bubble. With the passage of injection time, the cryogenic jet flow continues to squeeze the bubbles, resulting in a consecutive deformation of the ullage bubble in both axial and radial directions, as shown in Fig. 14b–d. However, the cryogenic jet flow does not penetrate through the ullage bubble. In spite of the little change of ullage shape and position, the temperature in the tank, especially inside the ullage bubble, rises to a relative high value (shown in Fig. 14d). Besides, the cryogenic jet fluid is difficult to flow over the ullage bubble and just stays in the top region of the tank, which is unfavorable for suppressing the thermal stratification in a tank.

Figure 15 shows the contours of the phase and temperature distribution changing with cryogenic jet injection time for the incident mass flow rate of 0.07 kg/s. It can be seen that the cryogenic jet fluid reaches the gas–liquid interface in about 13 s and penetrates little distance into the ullage bubble. At the time of 73 s, the cryogenic jet fluid runs through the ullage bubble, forming a cryogenic column region around the axis of the tank. Meanwhile, the temperature in the penetrated bubbles gradually increases due to the transferred heat from the wall. As the injection time goes on, the ullage bubble becomes deformed significantly, and even small bubbles are generated and run to the bottom of the tank, as shown in Fig. 15c. When the injection time lasts for about 303 s, more new bubbles appear near the bottom of the tank and grow gradually, whereas the main ullage bubble region still remains at the center of the tank. However, the original thermal stratification in the tank has been significantly destroyed. The temperature in the ullage bubble region is higher than that of the surrounding liquids, and the axis region is the coolest, as shown in Fig. 15d.

Figure 16 shows the contours of the phase and temperature distribution changing with cryogenic jet injection time for a given incident mass flow rate of 0.14 kg/s. It can be seen that, just as in the case 8 with mass flow rate of 0.07 kg/s, the cryogenic jet fluid arrives, penetrates and runs through the ullage bubble when the jet injection time lasts for about 6 s, 26 s and 56 s, respectively. As shown in Fig. 16 a to c, the main ullage bubble always remains at the center of the tank, excepting that slight deformation takes place gradually. Especially in Fig. 16c, the ullage bubble is penetrated through and generates long bubble tail towards the bottom of the tank. When the injection time lasts for 196 s, the shape of the ullage bubble is significantly deformed and new bubbles near the bottom of the tank grow larger. The entire axis region in the tank is occupied by the cryogenic fluid from the jet nozzle. From the Fig. 16d we can found that the thermal stratification in the tank, which is obtained from the first numerical simulation stage, has been significantly mixed. The temperature in the ullage bubble region is higher than that of the liquids surrounding it.

From the above investigation for the filling ratio of 78% we can found that a relatively large mass flow rate can penetrate the ullage bubble with the ullage position remains unchanged, which is similar to the cases with the filling ratio of 87%. In contrast, a larger filling ratio corresponds to a shorter jet time scale. With the passage of time, there is an increase of temperature in the ullage bubble, despite the ullage bubble stays at the center of the tank. In order to quantitatively analyze the influence of incident mass flow rate on the evolution of temperature and two-phase flow field, the relations between the temperature, pressure, velocity, mass of evaporation and the incident flow mass are shown in Fig. 17.

As shown in Fig. 17a, with increasing incident fluid mass, the average temperature increases rapidly at first, then remains stable for a while, and climbs gradually up finally. It is notable that the upward trend for the case of small mass flow rate of 0.035 kg/s is more evident than those for the other two cases. It is because in this case of 0.035 kg/s flow rate the cryogenic jet flow cannot penetrate through the ullage bubble, and the effect of the cryogenic jet for suppressing the thermal stratification in the tank is comparatively weaker. For the same mass of incident fluid, a higher incident mass flow rate corresponds to a lower average temperature of the tank, which is related to the fact that high incident mass flow rate can quickly deform the gas phase distribution inside the tank and promotes stronger convection and mixture process of the hot and cold liquids. The average velocity and pressure (shown in Fig. 12b, c) in the tank show similar trends as compared with the corresponding case with the filling ratio of 87%, in which the average velocity increases and the average pressure declines with the increase of incident mass flow rate. This means larger incident mass flow rate is more efficient to reduce the pressurization. Figure 12d depicts the relationship between evaporation and incident fluid mass. It can be found that the mass of evaporation gradually drops with increasing incident fluid mass. However, when the incident fluid mass is greater than 7 kg or so, the mass of evaporation begins to fluctuate, and in the case with the mass flow rate of 0.14 kg/s even shows an upward trend due to the rising of temperature inside the ullage bubble.

Through numerical investigation of the temperature destratification and the ullage bubble deformation influenced by cryogenic jet injection at the filling ratio of 98%, 87% and 78%, it is found that higher incident mass flow rate is more effective to promote the fluid flow in the tank and also more efficient to reduce the mass transfer caused by evaporation and condensation for a given liquid filling ratio, that is to say, more effective to suppress the thermal stratification in the tank.

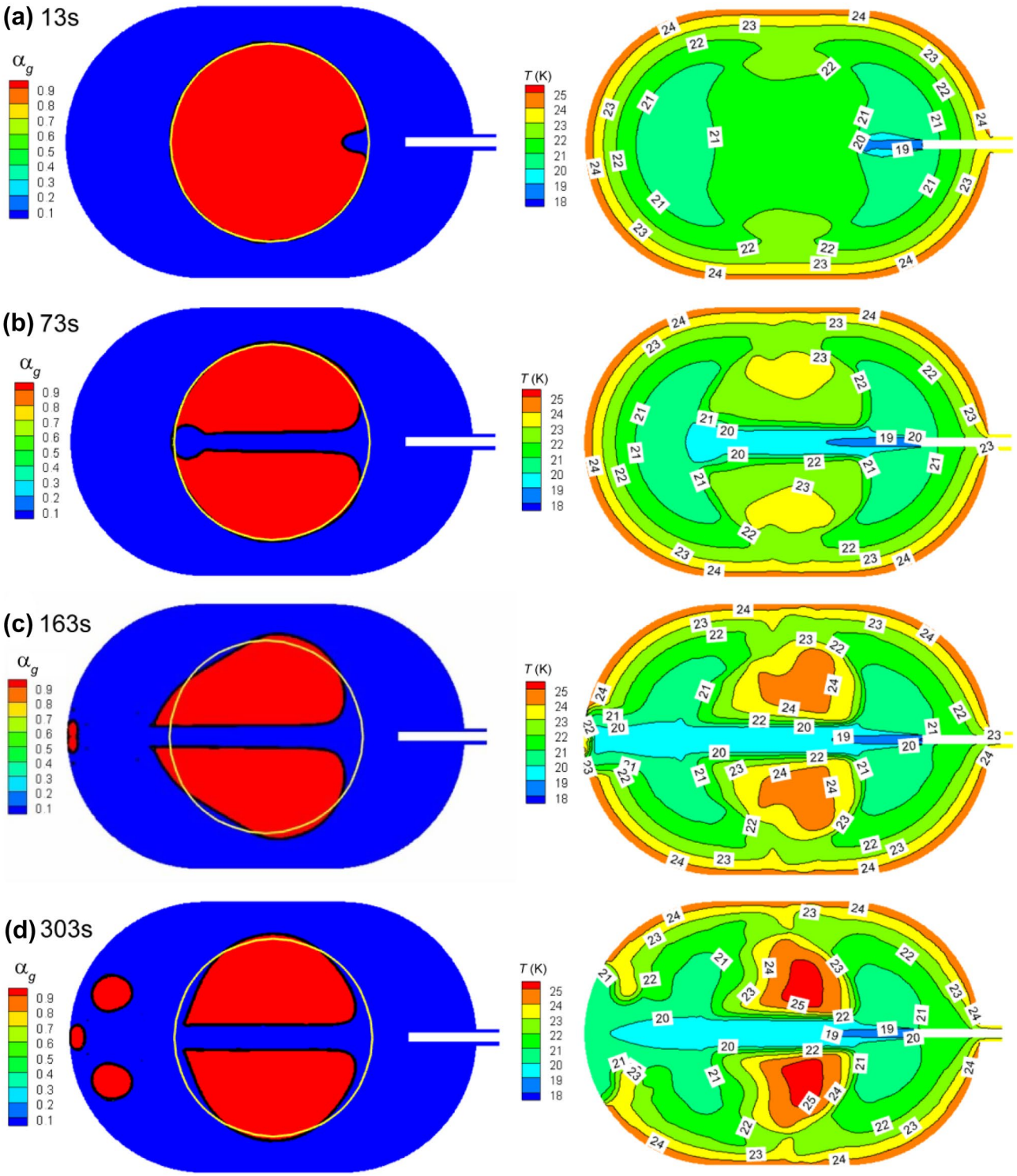

Fig. 15 Time evolution of contours of phase and temperature distribution for case 8

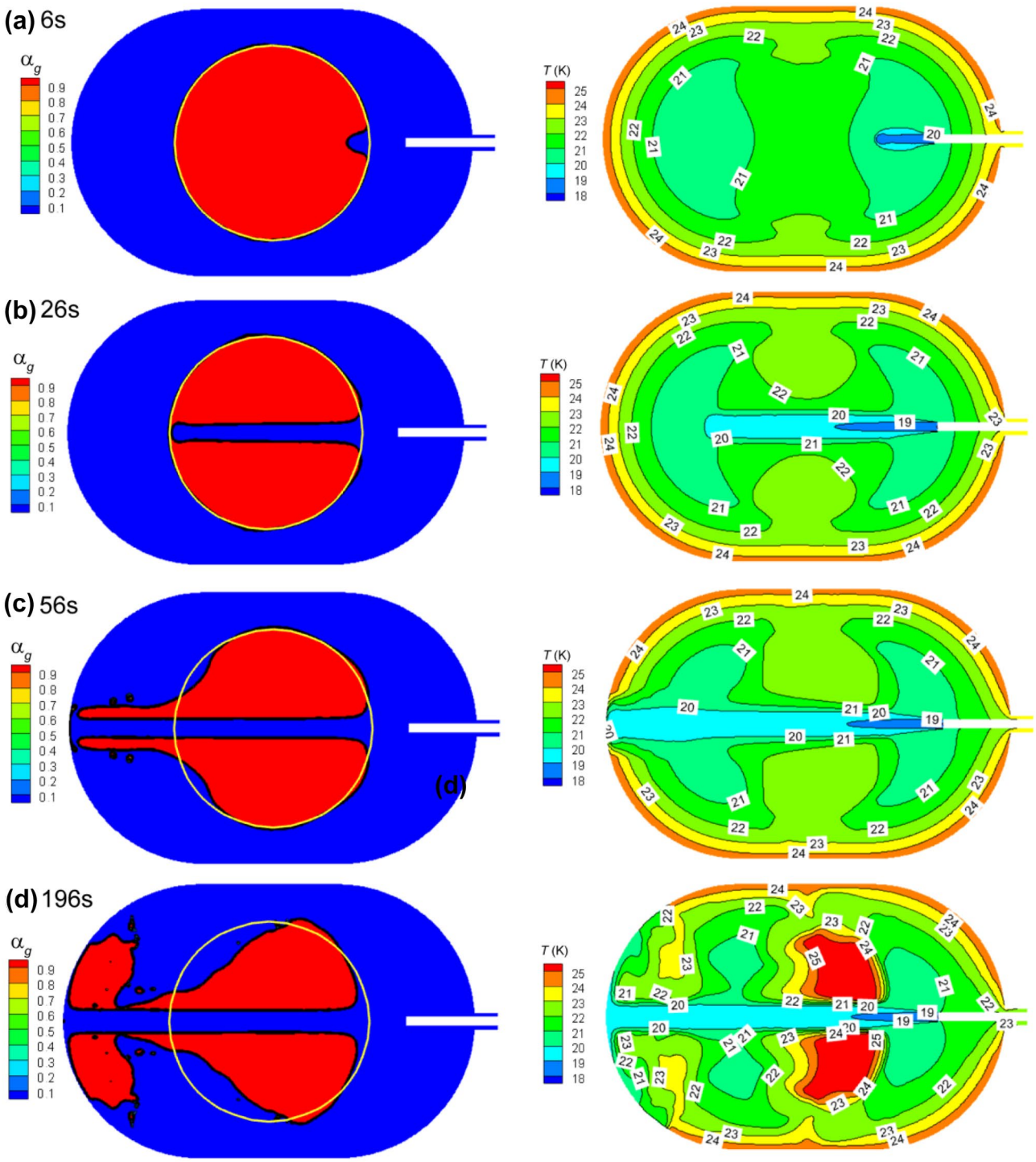

Fig. 16 Time evolution of contours of phase and temperature distribution for case 9

Influence of Filling Ratio

As seen in the aforementioned analyses, the mass flow rate plays a key role in the suppression of thermal stratification. However, the liquid filling ratio is also a necessary factor to be taken into consideration in view of the vital role the ullage bubble plays in the evolution of cryogenic jet flow in the tank. Therefore, a comparative study is carried out to analyze the influence of liquid filling ratio on the selected parameters of average temperature, pressure, velocity and the mass of evaporation.

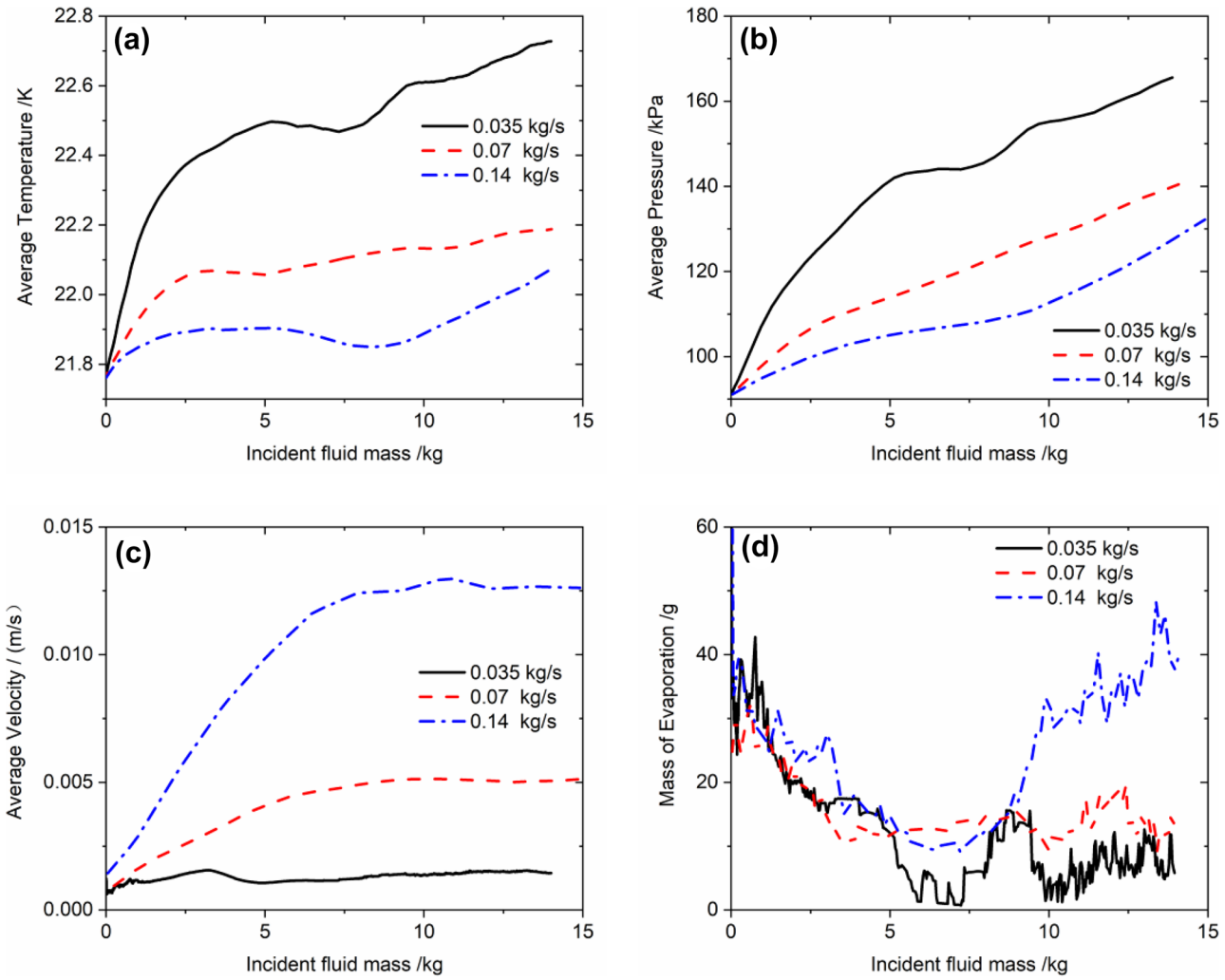

Fig. 17 Physical properties averaged over the tank versus incident fluid mass at 78% filling ratio

(1) Mass Flow Rate of 0.035 kg/s

Figure 18 shows the time evolution of physical variables in the tank when the incident mass flow rate is 0.035 kg/s. When the liquid filling ratio is 98%, it can be seen that the average temperature (Fig. 18a) inside the tank declines slightly, the average pressure (Fig. 18b) and the mass of evaporation (Fig. 18d) keep stable, and the average velocity (Fig. 18c) gradually increases with the passage of cryogenic jet injection time. When the liquid filling ratios are down to 87% and 78%, the average temperature, pressure and velocity increase slightly with the passage of injection time. The mass of evaporation remains small with fluctuation after a relatively rapid drop at the beginning of the cryogenic jet injection. This is consistent with the time evolution of average temperature which determines the amount of evaporation according to Eq. (8) of the phase change model. With the decrease of liquid filling ratio, the value of average temperature, pressure and mass of evaporation increase significantly. However, the average velocity, which is basically determined by the mass flow rate into the tank, shows little difference. The increase of average velocity for the filling ratio of 87% at the end of cryogenic jet injection (as shown in Fig. 18c) is due to the generated tiny bubbles moving around in the tank in this stage (as shown in Fig. 9d).

(2) Mass Flow Rate of 0.07 kg/s

Figure 19 shows the time evolution of physical variables in the tank with the incident mass flow rate of 0.07 kg/s. When the liquid filling ratio is 98%, it can be seen that the average temperature (Fig. 19a) inside the tank declines slightly, the average pressure (Fig. 19b) and the mass of evaporation (Fig. 19d) keep stable, and the average velocity (Fig. 19c) gradually increases with the passage of cryogenic

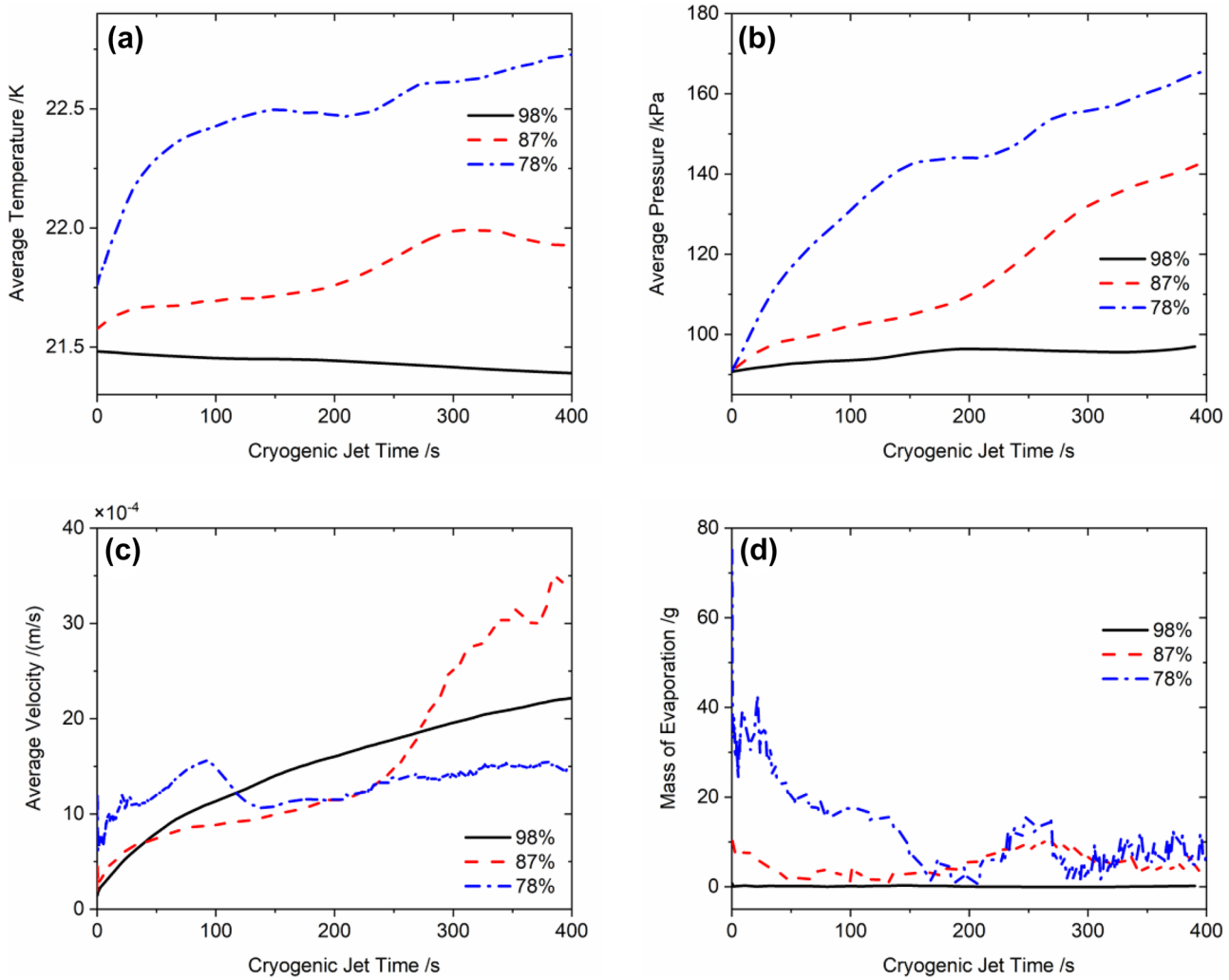

Fig. 18 Time evolution of physical variables averaged over the tank for mass flow rate of 0.035 kg/s

jet injection time. When the liquid filling ratios are down to 87% and 78%, the average temperature, pressure and velocity increase slightly with the passage of injection time. The mass of evaporation exhibits a relatively rapid drop at the beginning of the cryogenic jet injection, and then slightly fluctuates downward as the time passes. With decreasing liquid filling ratio, all the selected four physical variables manifest relatively high growth rates. Notably, at the end of cryogenic jet injection, the values of average velocity and the mass of evaporation for the filling ratio of 87% exceed that for the case of 78%, which is ascribed mainly to the generated tiny bubbles moving around in the tank in this stage (as shown in Fig. 9d).

(3) Mass Flow Rate of 0.14 kg/s

Figure 20 shows the time evolution of physical variables in the tank with the incident mass flow rate of 0.14 kg/s. When the liquid filling ratio is 98%, it can be seen that the average temperature (Fig. 20a) inside the tank declines slightly and the mass of evaporation (Fig. 20d) remains stable with weak fluctuation with the passage of cryogenic jet injection time. When the liquid filling ratios are down to 87% and 78%, the average temperature gradually rises up with a slight decrease at the beginning of the cryogenic jet injection. The mass of evaporation shows considerable fluctuation after a relatively rapid drop at the beginning of the cryogenic jet injection.

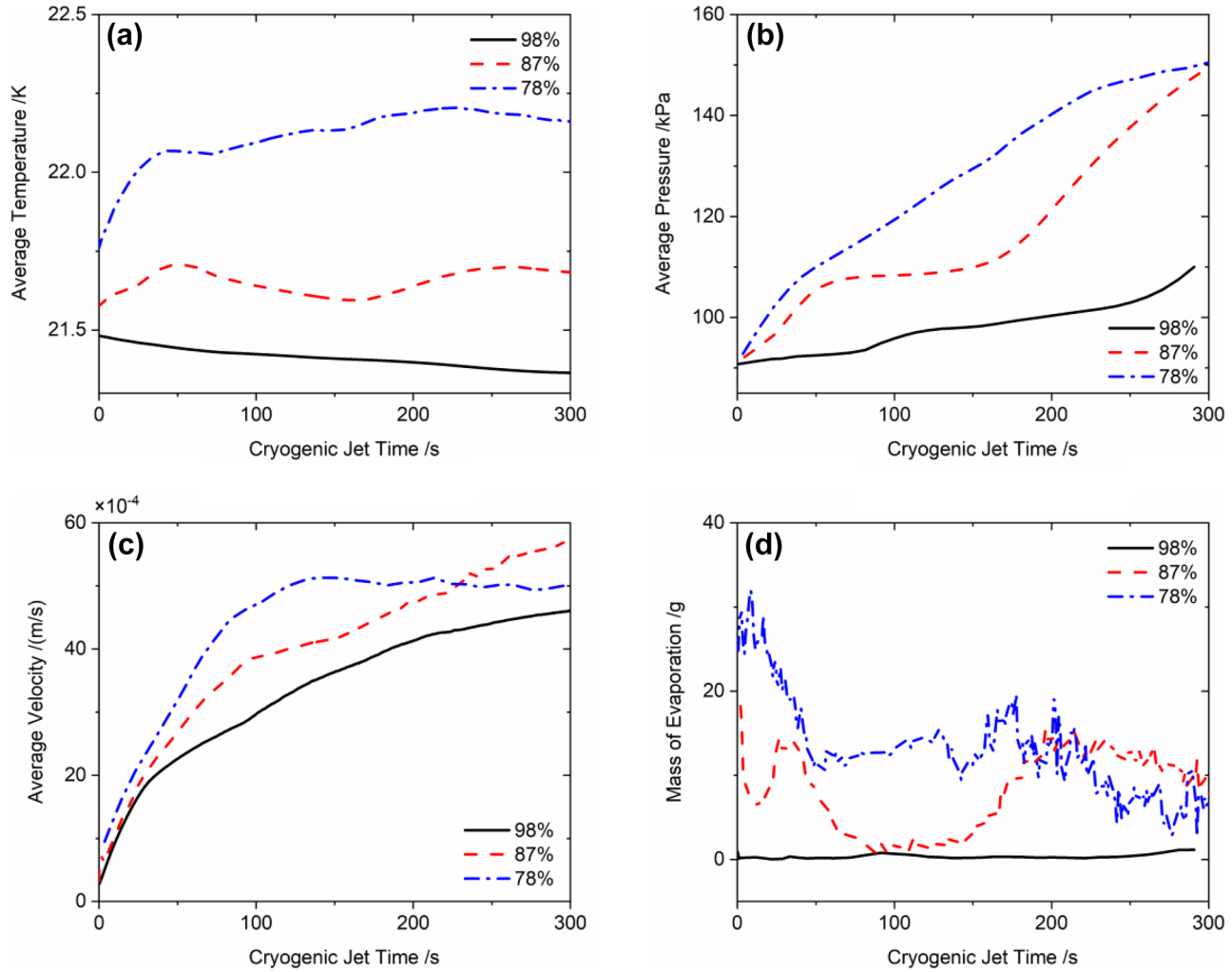

Fig. 19 Time evolution of physical variables averaged over the tank for mass flow rate of 0.07 kg/s

This is consistent with the time evolution of average temperature (shown in Fig. 20a) which determines the amount of evaporation according to Eq. (8) of the phase change model. For all the three different filling ratios, the average pressure (Fig. 20b) gradually grows up, and the average velocity (Fig. 20c) shows a rapid increase firstly and then remains steady with the passage of injection time. With the decline of liquid filling ratio, all the selected four physical variables manifest relatively high growth rates.

Through above analyses about the influence of liquid filling ratio on the selected parameters of average temperature, pressure, velocity and mass of evaporation, it is found that a smaller filling ratio, namely a larger proportion of gas phase, results in a faster growth of average temperature and pressure inside the tank during the process of cryogenic jet injection. Therefore, higher incident mass flow rate is required to suppress the growth rates of temperature and pressure. Besides, it is more efficient to suppress the thermal stratification when the liquid filling ratio is small inside a tank at a given incident mass flow rate. Furthermore, the mass transfer caused by evaporation and condensation is smaller for lower liquid filling ratio.

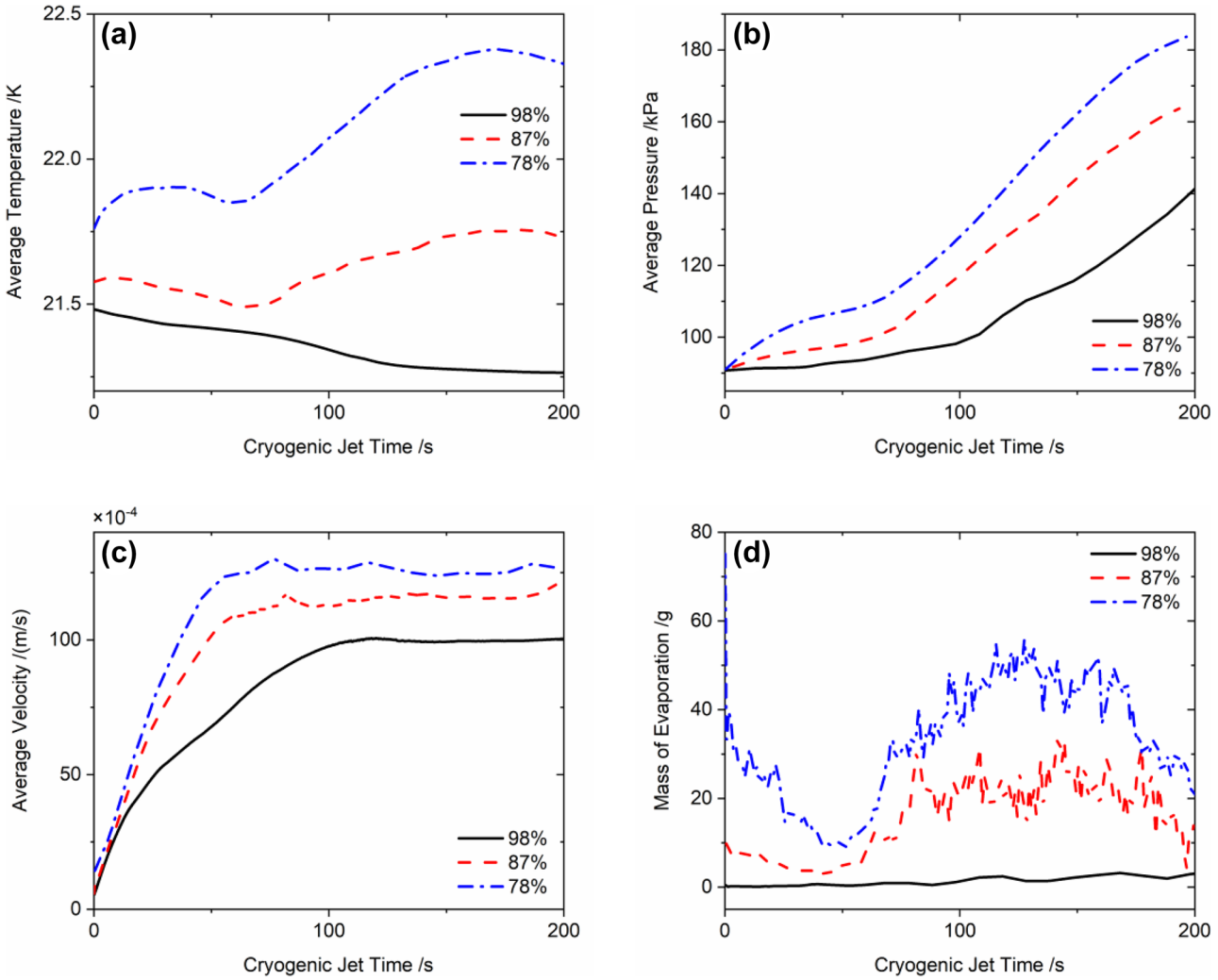

Fig. 20 Time evolution of physical variables averaged over the tank for mass flow rate of 0.14 kg/s

Conclusion

In the present study, the temperature stratification caused by heat leakage on the wall and its suppression are studied in the context of a partially filled large-scale liquid hydrogen storage tank. Evolution processes of the temperature destratification and the ullage bubble deformation in the tank during the injection of a cryogenic jet are analyzed and compared. And the effects on the suppression of temperature stratification by cryogenic jet are discussed for different mass flow rates and filling ratios. It is concluded that when the liquid filling ratio is constant, a higher incident mass flow rate destroys more effectively the temperature stratification inside the tank and produces a stronger inside fluid flow. For a given mass flow rate, a smaller filling ratio, namely a larger proportion of gas phase, results in a faster growth of the average temperature and pressure, and a larger amount of mass transfer inside a tank during the injection of cryogenic jet. Therefore, on one hand, higher incident mass flow rate is required to reduce the mass transfer caused by evaporation and condensation and to suppress the thermal stratification in the tank. On the other hand, the effect of destratification is stronger when the liquid propellant filling ratio is large, namely at the beginning of the system operation when the propellant has not been used two much.

Acknowledgements This research is supported by the Key Research Program of Frontier Sciences, CAS (Grant No. QYZDY-SSW-JSC040) and the National Nature Science Foundation of China (Gant No. 12172363, 11672311).

Funding Key Research Program of Frontier Sciences,CAS,QYZDY-SSW-JSC040,Kai Li,National Natural Science Foundation of China,12172363,Kai Li,11672311,Kai Li

Data availability The datasets generated and analyzed during the current study are available from the corresponding author on reasonable request.

Declarations

Conflicts of interest The authors declare no conflict of interest.

References

Aydelott, J.C.: Normal gravity self-pressurization of 9-inch-(23 cm) diameter spherical liquid hydrogen tankage. NASA TN-D-4171 (1967a)

Aydelott, J.C.: Effect of gravity on self-pressurization of spherical liquid-hydrogen tankage. NASA TN-D-4286 (1967b)

Aydelott, J.C.: Effect of size on normal-gravity self-pressurization of spherical hydrogen tankage. NASA TND-5196 (1969)

Barnett, D.O., Mcreynolds, L .S., Winstead, T.W.: An investigation of liquid-hydrogen stratification in a large cylindrical tank of the saturn configuration. (1965)

Barsi, S., Kassemi, M.: Numerical and experimental comparisons of the self-pressurization behavior of an LH2 tank in normal gravity. Cryogenics **48**, 122–129 (2008)

Brackbill, J.U., Kothe, D.B., Zemach, C.: A continuum method for modeling surface tension. J. Comput. Phys. **100**(2), 335–354 (1992)

Grayson, G., Lopez, A., Chandler, F., Hastings, L., Brethour J.: CFD modeling of helium pressurant effects on cryogenic tank pressure rise rates in normal gravity. 43rd AIAA/ASME/SAE/ASEE Joint Propulsion Conference & Exhibit. (2007)

Guo, B., Zhao, J.F., Li, K., Hu, W.R.: Thermal destratification in hydrogen propellant tank in space by jet injection. Chinese Journal of Space Science. **40**, 1052–1065 (2020)

Guo, B., Zhao, J.F., Li, K., Hu, W.R.: Numerical study on thermal destratification in large scale hydrogen propellant tank in space by jet injection under zero gravity condition. Chinese Journal of Theoretical and Applied Mechanics. **53**, 1170–1182 (2021)

Hasan, M.M., Lin, C.S., Van Dresar, N.T.: Self-pressurization of a flight weight liquid hydrogen storage tank subjected to low heat flux. ASMWAICHE National Heat Transfer Conference. (1991)

Hastings, L.J., Plachta, D.W., Salerno, L., Kittel, P.: An overview of NASA efforts on zero boil off storage of cryogenic propellants. Cryogenics **41**, 33–839 (2001)

Hochstein, J.I., Ji, H.C., Aydelott, J.C.: Effect of subcooling on the on-orbit pressurization rate of cryogenic propellant tankage. AIAA/ASME 4th Joint Thermo-physics and Heat Transfer Conference. Boston, Massachusetts, AIAA. (1986)

Hochstein, J.I., Ji, H.C., Aydelott, J.C.: Prediction of self-pressurization rate of cryogenic propellant tankage. J. Propul. Power **6**, 11–17 (1990)

Kassemi, M., Kartuzova, O., Hylton, S.: Validation of two-phase CFD models for propellant tank self-pressurization: crossing fluid types, scales, and gravity levels. Cryogenics. **89** (2017)

Lee, W.H.: A pressure interation scheme for two-phase modeling. Technical Report LA-UR 79–975 Los Alamos Scientific Laboratory, Los Alamos, New Mexico, (1979)

Li, J.C., Lin, H., Zhao, J.F., Li, K., Hu, W.R.: Dynamic behaviors of liquid in partially filled tank in short-term microgravity. Microgravity Sci. Technol. **30**, 849–856 (2018)

Li, J.C., Lin, H., Li, K., Zhao, J.F., Hu, W.R.: Liquid sloshing in partially filled capsule storage tank undergoing gravity reduction to low/micro-gravity Condition. Microgravity Sci. Technol. **32**, 587–596 (2020a)

Li, J.C., Lin, H., Li, K., Zhao, J.F., Hu, W.R.: Dynamic behavior in a storage tank in reduced gravity using dynamic contact angle method. Microgravity Sci. Technol. **32**, 1039–1048 (2020b)

Lin, C.S., Van Dresar, N.T., And Iiasan, M.M.: A pressure control analysis of cryogenic storage systems. AlAA Paper 91–2405 (1991)

Lin, C.S., Hasan, M.M.: Self-pressurization of a spherical liquid hydrogen storage tank in a microgravity environment. NASA TM 105372 (1992)

Ma, Y., Sun, P.J., Li, P., Li, Y.Z., Wang, L.: Numerical investigation on performance of spraying pressure control technique for liquid hydrogen tank at microgravity. Vacuum and Cryogenics. **24**, 266–274 (2018)

Ma, Y., Li, Y., Zhu, K., Wang, Y., Wang, L., Tan, H.: Investigation on no-vent filling process of liquid hydrogen tank under microgravity condition. Int. J. Hydrogen Energy **42**, 8264–8277 (2017)

Schmidt, A.P., Purcell, J.R., Wilson, W.A., Smith, R.V.: An experimental study concerning the pressurization of liquid hydrogen. Journal of research of the National Bureau of Standards. **65**, 2 (1961)

Schepper, D., Sandra, C.K., Geraldine, J.: Modeling the evaporation of a hydro-carbon feedstock in the convection section of a steam cracker. Comput. Chem. Eng. **33**(1), 122–132 (2009)

Wang, L., Li, Y., Li, C., Zhao, Z.: CFD investigation of thermal and pressurization performance in LH2 tank during discharge. Cryogenics **57**, 63–73 (2013a)

Wang, L., Li, Y., Zhao, Z., Liu, Z.: Transient thermal and pressurization performance of LO2 tank during helium pressurization combined with outside aerodynamic heating. Int. J. Heat Mass Transf. **62**, 263–271 (2013b)

Zuo, Z.Q., Sun, P.J., Jiang, W.B., Qin, X.J., Li, P., Huang, Y.: Thermal stratification suppression in reduced or zero boil-off hydrogen tank by self-spinning spray bar. Int. J. Hydrogen Energy **44**, 20158–20172 (2019)